DEPARTMENT OF DEFENCE
DEFENCE SCIENCE & TECHNOLOGY ORGANISATION
DSTO

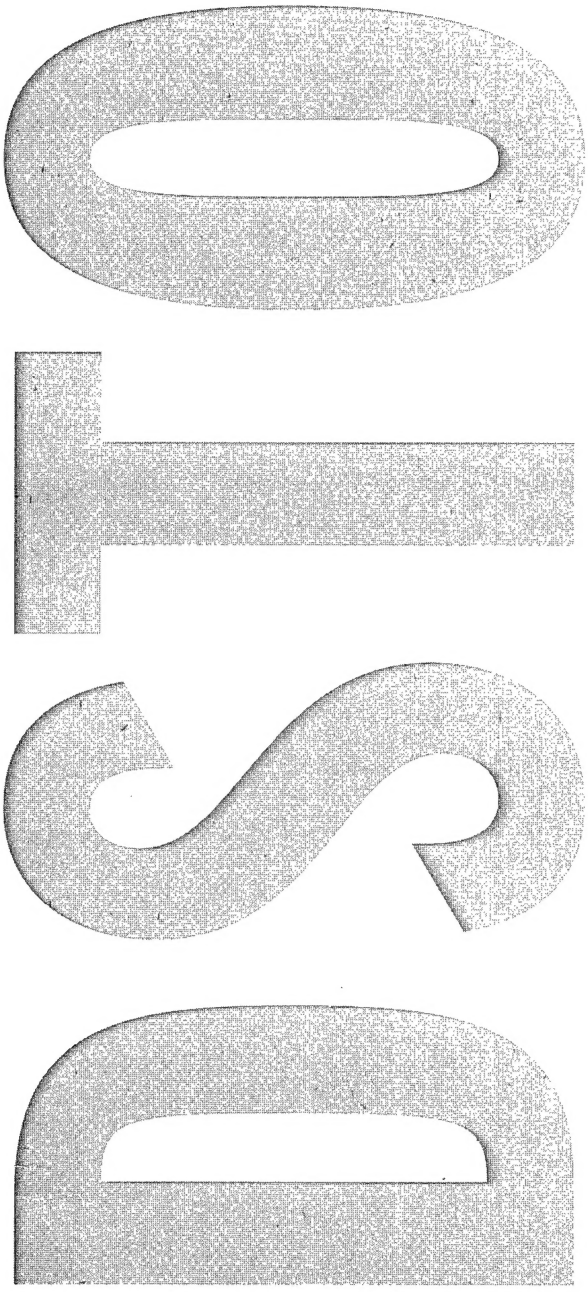

Microgrid Plastic Strain Analysis of a Representative F-111C Fuel Flow Vent Hole 13 Coupon

E. Kowal and M. Heller

DSTO-TR-0951

Microgrid Plastic Strain Analysis of a Representative F-111C Fuel Flow Vent Hole 13 Coupon

E. Kowal and M. Heller

Airframes and Engines Division
Aeronautical and Maritime Research Laboratory

DSTO-TR-0951

ABSTRACT

This report presents results for the application and associated improvement of an AED microgridding procedure for the determination of highly localised strains. The procedure has been applied to determine plastic strains at the critical location for a plate with a reworked FFVH13 geometry, subjected to F-111C CPLT loading. By using multiple measurements over an increased gauge length of 150 μm, highly accurate strains, ranging in accuracy between 57 and 135 micro strain were determined. This accuracy level is approximately an order of magnitude better than the prior microgridding approach. For the critical region, detailed non-linear strain hysteresis responses were obtained, and the measured peak and residual strains of -2.16024% strain and -0.79349% strain respectively agreed well with prior finite element predictions. The measured residual compressive strains at the critical location indicate that there is a significant residual tensile stress, which is consistent with the known occurrence of fatigue cracking in the fleet. This investigation has also provided valuable strain data for use in validating advanced FE based constitutive models, which are currently used and under development in AED for obtaining airframe structural integrity assessments.

Published by

DSTO Aeronautical and Maritime Research Laboratory
PO Box 4331
Melbourne Victoria 3001 Australia

Telephone: (03) 9626 7000
Fax: (03) 9626 7999

AR-011-236
March 2000

APPROVED FOR PUBLIC RELEASE

Microgrid Plastic Strain Analysis of a Representative F-111C Fuel Flow Vent Hole 13 Coupon

Executive Summary

In recent years AMRL has been tasked by the Royal Australian Air Force (RAAF) to undertake investigations relating to life assessment and life extension for the F-111C airframe. Particular emphasis has been directed at the wing pivot fitting, which contains a large number of machined elongated fuel flow vent holes, where FFVH13 in particular is critical. Currently fatigue cracking at these holes is being managed by reworking the elongated fuel flow vent holes to a family of progressively larger shapes. Durability and damage tolerance analysis (DADTA) are required to determine safe inspection intervals for FFVH13 for the range of rework configurations, and here a detailed knowledge of the severity of the local stress and strain responses is a key input. The stresses are typically determined from detailed FE analyses, which are validated through comparison with selected measured strains from both full scale and specimen tests. In prior investigations, FE analysis has been undertaken to compare predicted plastic strains, with strain gauge data obtained from a full scale wing test and specimen tests and there has been some lack of correlation. This is believed to be due to a lack of strain gauge reliability under very-high-strain, low-cycle loading. In the present work the suitability of an Airframes and Engines Division (AED) microgrid strain measurement technique to determine accurate strains for the F-111C context of an elongated FFVH13 is considered.

This report presents results for the application and associated improvement of an AED microgridding procedure for the determination of highly localised strains. The procedure has been applied to determine plastic strains in the critical location for a plate with a reworked FFVH13 geometry, subjected to F-111C Cold Proof Load Test (CPLT) loading. By using multiple measurements over a gauge length of 150 μm, highly accurate strains ranging in accuracy between 57 and 135 micro strain were determined. This accuracy level is approximately an order of magnitude better than the prior microgridding approach. For the critical region, detailed non-linear strain hysteresis responses were obtained, and the measured peak and residual strains of -2.16024% strain and -0.79349% strain respectively agreed well with prior finite element predictions. The measured residual compressive strains at the critical location indicate that there is a significant residual tensile stress at the critical location, which is consistent with the known occurrence of fatigue cracking in the fleet.

This work has provided AED with a significantly improved capability in determining accurate strain measurements, and this has particular benefits for obtaining accurate structural integrity assessments of RAAF structural components, such as the F-111C airframe.

Authors

E.Kowal

Airframes and Engines Division

Eva Kowal graduated from the University of Newcastle-upon-Tyne (UK) in 1972 with a B.Sc. degree (joint honours in Botany and Genetics). In 1988 she obtained a B.App.Sc. in Scientific Photography from RMIT, Melbourne. During 1973-1977 she was involved in microscopy and botanical anatomy at the University of N.S.W., Sydney. She then worked for the NSW Department of Agriculture during 1977-1980, involved in identifying anatomical features of merino sheep which confer resistance to fleece rot and blowfly strike. During 1980-1988 she was employed as the Divisional Photographer at CSIRO, Division of Mineral Products, Melbourne. Since 1988 she has worked at AMRL, involved in; fractography; the development of a microgridding technique to measure low strains; and its application to the study of fatigue of materials and associated components.

M. Heller

Airframes and Engines Division

Manfred Heller completed a B. Eng. (Hons) in Aeronautical Engineering at the University of New South Wales in 1981. He was awarded a Department of Defence Postgraduate Cadetship in 1986, completing a PhD at Melbourne University in 1989. He commenced work inStructures Division at the Aeronautical Research Laboratory in 1982. He has an extensive publication record focussing on the areas of stress analysis, fracture mechanics, fatigue life extension methodologies and experimental validation. Since 1992 he has led tasks which develop and evaluate techniques for extending the fatigue life of RAAF aircraft components and provide specialised structural mechanics support to the RAAF. He is currently a Senior Research Scientist in the Airframes and Engines Division.

Contents

Notation

μm	micron
mm	millimetre
cm	centimetre
kN	kilonewton
X,Y,Z	global cartesian co-ordinates
A	co-ordinate origin
B	critical stress location
ρ	correlation coefficient
L	gauge length
Y	linear values for the corresponding probability scale
n	number of readings
ε	percentage strain
σ	standard deviation

Subscripts

i	individual reading
L	gauge length
Y	linear values for the corresponding probability scale
ε	percentage strain

List of Abbreviations

AMRL	Aeronautical & Maritime Research Laboratory
AED	Airframes and Engines Division
RAAF	Royal Australian Air Force
CPLT	Cold Proof Load Test
DADTA	Durability and Damage Tolerance Analysis
FFVH	Fuel Flow Vent Hole
FFVH13	Fuel Flow Vent Hole number 13
FE	Finite element
CCD	Charged coupled device

1. Introduction

AMRL has been tasked by the Royal Australian Air Force (RAAF) to undertake investigations relating to life assessment and life extension for the F-111C airframe. Particular emphasis has been directed at the wing pivot fitting, which is manufactured from D6ac steel, and has some fatigue critical locations. For example, the wing pivot fitting contains a large number of machined elongated fuel flow vent holes (FFVH), as shown in Figure 1. It is well known that under Cold Proof Load Tests (CPLT), and high service loads, the material around one of these holes, FFVH13, experiences extensive plastic deformation which results in the introduction of residual tensile stresses. These residual stresses coupled with the local response to the in-service flight loading are detrimental, and contribute to crack initiation and growth at the lower inboard corner.

Currently, the problem is being managed by reworking the elongated fuel flow vent holes to a family of progressively larger shapes [1,2]. This process removes small cracks and corrosion as detected. The extent of the rework depends on the size of the detected crack. Durability and damage tolerance analyses (DADTA) are required to determine safe inspection intervals for FFVH13 for the range of rework configurations in the RAAF fleet. Here a detailed knowledge of the severity of the local stress and strain responses is a key input to the DADTA process. The stresses are typically determined from detailed FE analyses, which are validated through comparison with selected strain data from both full scale and specimen tests. Hence for this purpose, accurate experimental determination of strains under plastic deformation conditions is a key requirement.

In prior investigations, FE analysis of a FFVH13 substructure model, for the CPLT load sequence, has been undertaken to compare predicted plastic strains, with strain gauge data obtained from a full scale wing test [3]. The FE predictions have shown some lack of correlation with strain gauge data. In addition, FE modelling of a plate specimen with an elongated hole for the CPLT loading sequence has been used to simulate the plastic strains at the critical stress location at FFVH13 [4]. These predictions have been compared to experimental results for a strain gauged plate containing the elongated hole. However, these results also show some lack of correlation. In these two FE studies, the lack of correlation with strain gauge data is at least partially explained by poor strain gauge reliability under very-high-strain, low-cycle loading. This is believed to be due primarily to the degradation of the adhesive, (and hence strain readings) used to bond strain gauges for these conditions. Other experiments, comparing extensometer and strain gauge data, have also cast serious doubt on the reliability of strain gauge results under very-high-strain, low-cycle loading conditions [5].

Hence, it was decided in the present work to investigate the potential of the AED microgrid strain measurement technique [6] to determine accurate strains for the F-111C context of an elongated FFVH13. In the microgrid method, local strains can be determined by measurement of displacements of grid points on test specimens during loading. Using photographic techniques, a square grid of lines with 25 μm pitch is applied to the surface of a specimen. As the specimen is loaded, photographs of the

deformed grid are taken for the subsequent microscopic analysis. The microgrid measurement system, based on a 25 μm gauge length, has a standard error of approximately 3,000 micro strain [6, 7]. The standard error is defined here as the standard deviation of the mean. Given the high standard error for a 25 μm gauge length, this system has historically been considered suitable only for problems involving extremely high plasticity, as is the case for crack tips. However, by incorporating some changes to the procedure, the aim is to obtain significant improvements in accuracy of measured strains, and apply it to determine plastic strain responses for the FFVH13 coupon specimen. The key difference to previous microgridding work is that multiple readings are made, and the gauge length has been increased from 25 μm to 150 μm.

In Sections 2 and 3, descriptions of the specimen configuration and the experimental method are respectively given. This is followed in Section 4 with the method for analysis of the measured data. The strain results, including estimates of strain accuracy are then given in Section 5, followed by conclusions in Section 6.

2. Test Specimen

2.1 Specimen geometry and preparation

The geometry for the test specimen manufactured from D6ac steel is shown in Figure 2. The plate was 76.3 mm wide, 245 mm long and had a thickness of 5 mm. The hole in the plate was 50.8 mm long and 25.4 mm wide and its major axis is oriented at an angle of 16 degrees relative to the remote loading axis. The size and orientation of the oversized elongated hole has been chosen to be the same as that used in prior strain investigations [4], where strain gauge measurements were compared to predictions from non-linear finite element analyses. It is also the same as the rework size for an interference fit life extension option under development at AMRL [10]. The hole orientation of 16^{o} has been used in the present and preceding work, to locate the maximum hoop stress at the hole edge, in the same position as determined for an actual representative geometry and loading of the FFVH13 in the wing pivot fitting [1].

Prior to application of micro grids the specimen was polished using kerosene as a lubricant in the following sequence, (i) P800 silicon carbide abrasive paper, (ii) P1000 silicon carbide abrasive paper, (iii) 15 μm diamond paste on silk cloth, (iv) 1 μm diamond paste on rayon cloth with short nap. Square microgrids (25 μm pitch) were applied using a photoresist method to the elongated hole area on one side of the specimen covering an area of 7 x 7 cm. The method used has been described in detail in prior work [6]. However in the present investigation, two changes were made, namely: the photoresist used was Hoechst AZ 1518 DG and the developer was Hoechst AZ 400K.

2.2 Location of measurement areas

The global cartesian co-ordinate system used for defining the location of the region of interest is shown in Figure 3. Here point A is the designated coordinate origin and point B is the critical stress location at the hole edge where Y = +15.70 mm. An enlargement of the region in the vicinity of Point B is given in Figure 4. Here the 5 measurement areas selected for analysis are shown, where each area represents a 7 by 7 array of grids, as shown in Figure 5. For each 7 x 7 grid the spacing pitch was 25 μm, and, the distances 1A, 4D and 7G represent three gauge lengths, each nominally 150 μm. The point "O" on each 150 μm gauge length is located in the specimen X-Y axis system with reference to the global origin. The point "X" in each of the 5 measurement areas is located in the specimen global X-Y system as listed in Table 1. Areas 1, 2 and 3 do not have the same Y coordinate and areas 1, 4 and 5 do not have the same X coordinate because the exact location of the 5 measurement areas is based on the selection of good quality grids. The point "X" represents the centre (point "O") of gauge 7G in each of the measurement areas (Figure 5). Table 2 lists the coordinates at point "O" for the 3 gauge lengths at the 5 measurement areas.

3. Experimental Method

Uniaxial testing of the specimen was undertaken using a 300 kN servohydraulic machine (MTS1). The following representative F-111C loading was applied to the specimen, (i) a CPLT sequence of 0, 138, -252, 138, -252 and 0 kN, followed by (ii) a sample spectrum loading of +80, 0, -80 and 0 kN. The sequence of the representative loading is shown schematically in Figure 7. At each increment of the load sequence, a photographic recording of the deformed microgrids was made, for each of the five measurement areas, to enable subsequent strain analysis to be undertaken. The key difference to previous microgridding work is that multiple readings are made, and that the gauge length has been increased from 25 μm to 150 μm.

3.1 Photographic recording of measurement areas

The equipment used for the photographic recording of the selected microgridded areas during loading is shown in Figure 6. The equipment consisted of a modified Olympus metallurgical microscope mounted on a X-Z traversing stage having a coordinate measurement and display capability. The microscope was equipped with a 35 mm camera, a X20 objective lens and reflected lighting. The total grid magnification on the film was determined, after completion of testing, to be 76.03 by comparing the known undeformed gauge length of 150 μm to the measured length. The modular construction of the microscope permitted it to be reassembled such that the optical axis was horizontal instead of its former vertical orientation. This horizontal orientation of the optics enabled the surface of the microgridded specimen in the test machine to be observed and photographed.

The modified microscope was bolted onto a custom-made traversing stage fitted with linear measurement gauges and digital display. This allowed precise positioning of the microscope in order to locate the selected areas in the critical stress location on the specimen. The traversing stage had movement in the X and Z directions (corresponding respectively to the X and Y axes on the specimen). Movement in the X direction was controlled manually by rotation of the handwheel. However, torque properties of the Z column necessitated that the Z column be motorised in order to facilitate focussing on the 25 μm microgrids (at the X76.03 magnification used, the optical focussing tolerance was only 3 μm). Movement in the Z direction was thus controlled electronically by the activation of stepper motor drives allowing movement in the range 2 - 600 μm per second.

Prior to any loading of the specimen, the five selected areas in the critical stress zone were photographed on black/white film (Kodak techpan) at zero load and the coordinates representing point "X" were recorded (Table 1). Subsequently photographs at each load in the sequence were made.

3.2 Measurement of 150 μm gauge lengths

As noted in the preceding Section 3.1, the original nominal 150 μm gauge length has been magnified to 11,400 μm on the film. To accurately determine deformations the now 11,400 μm gauge lengths on the film were viewed at a magnification of X30. This was achieved using a Zeiss microscope with transmitted illumination, using the associated instrumentation as shown in Figure 8. The microscope was fitted with a CCD video camera and a moveable stage with digital X and Y direction micrometers. The stage was used to move the negative (and hence the image on the video monitor) until the desired grid point was under the set of cross hairs drawn on the monitor screen. The Y position coordinates of the grid points on the enlarged nominal 11,400 μm gauge length were read from the digital micrometers, which had a resolution of 1μm. Finally, the measured gauge lengths were divided by 76.03 thereby adjusting the measurements back to a nominal 150 μm. The resulting measurements of the nominal 150 μm gauge lengths were significant to two decimal places.

Twenty repeat measurements were taken in each of the three areas, for each gauge length 1A, 4D and 7G. The three gauges (1A, 4D and 7G) in area 1 were measured in the case of the CPLT sequence of 0, 138, 0, -252, 0, 138, 0, -252 and 0 kN. In addition, gauge 7G in area 1 was also measured in the case of the sample spectrum loading of 80, 0, -80 and 0 kN. The three gauges in area 3 were measured for the CPLT sequence only. The raw experimental readings for areas 1 and 3 at the various loading points are given in Appendices A and B respectively.

4. Analysis Method

In this section the equations used to determine the key quantities of interest are given, namely mean length, mean strain, standard deviation of the strain and strain accuracy.

Also the procedure to check the validity of the assumption that the data is normally distributed is given.

4.1 Raw measurements

The two extreme data points furthest from the mean were discarded for each set of 20 measurements and the remaining 18 measurements retained for analysis. In the Tables given in Appendices A and B, the 20 listed measurements have been reordered whereby, the first 18 measurements listed are those used in the analysis of the data.

4.2 Assessment of normality of data distribution

Prior to presenting any statistical determination of the mean, standard deviation or accuracy, it was necessary to assess whether the gauge length data (18 measurements) exhibited a normal distribution. This was done by analysing the normality of the data for one set of readings, namely gauge 7G in area 1 at load point 1, ie at 0kN. This set of 18 measurements for gauge 7G was plotted as shown in Figure 9; whereby, the vertical scale indicates the percentage of readings at or below the value of a particular gauge length. Here, the vertical ordinate spacings are arranged on a probability scale such that any set of data representing a normal distribution should plot as a straight line [9]. Hence the correlation coefficient, ρ_{LY}, of the gauge length measurements and the linear values on the right ordinate was next calculated, to indicate how well the data matched a desired linear behaviour using the following equation:

$$\rho_{LY} = \frac{\dfrac{\Sigma(L_i - \bar{L})(Y_i - \bar{Y})}{(n-1)}}{\sqrt{\left(\dfrac{\Sigma(L_i - \bar{L})^2}{(n-1)}\right)\left(\dfrac{\Sigma(Y_i - \bar{Y})^2}{(n-1)}\right)}} \tag{1}$$

where L_i are the gauge length readings, n is number of readings, Y_i are the linear values of the vertical axis given in Figure 9, and the superscript indicates the average of the n readings.

4.3 Calculation of average strain and standard deviation

Percentage strains were calculated from the changes in the nominal 150 μm gauge lengths during the F-111C representative loading for both areas 1 and 3 using the equation:

$$\bar{\varepsilon} = \left(\frac{\bar{L} - 150}{150}\right)100 \tag{2}$$

where $\bar{\varepsilon}$ is the average percentage strain and $\bar{L}$ is the average gauge length.

The standard deviation of the strain (in terms of % strain) was calculated as follows:

$$\sigma_\varepsilon = \sqrt{\frac{\Sigma(\varepsilon_i - \bar{\varepsilon})^2}{(n-1)}} \tag{3}$$

where σ_ε is the standard deviation of the strain and ε_i is the individual strain reading (both in terms of % strain).

4.4 Accuracy of the strain

The standard error, ie the standard deviation of the mean strain, $\sigma_{\bar{\varepsilon}}$, was used as an indication of accuracy of the mean for a set of readings for a particular gauge. The equation used is:

$$\sigma_{\bar{\varepsilon}} = \frac{\sigma_\varepsilon}{\sqrt{n}} \tag{4}$$

5. Results and Discussion

5.1 Statistical assessment of data

Using Equation (1) for the data plotted in Figure 9, it was found that the correlation coefficient was 0.99, indicating that the typical gauge length data can be assumed to be normally distributed. The fitted line is also plotted in Figure 9. The standard deviation for all data sets of 18 readings was determined using Equation (3) with the results for all load increments of areas 1 and 3 given in Tables 3 and 4 respectively. It can be seen that the data for all the gauges fall within ±2 standard deviations being consistent with the assumption of a normal distribution. Finally, the accuracy of the mean strain (defined as the standard deviation of the mean strain) for all data sets of 18 readings was evaluated using Equation (4). These results are also given in Tables 3 and 4. The individual accuracy values for gauges 1A, 4D and 7G range from 0.0057 to 0.0135 % strain (ie 57 to 135 micro strain), indicating that highly accurate strain values can be determined using the present approach.

5.2 Strains

5.2.1 Strains in area 1

The strain results for this area are summarised in Figure 10 (a) for each gauge, while Table 5 and Figure 11 give the average response for the gauges together. Strain hysteresis responses for gauges 1A and 4D during CPLT loading are given in Figures 12 to 13 respectively, while Figure 14 gives the response for gauge 7G for both the CPLT and the sample flight load. The corresponding area average strain response is given in Figure 15. From Figures 12 to 14, it can be seen that the strain response is elastic during the application and removal of the first tensile loading of 138 kN and that the elastic strains are similar for all 3 gauges. However, the high compressive loading to -252 kN causes material yielding, and upon its removal, residual compressive strains are induced which is reflected in the average negative strain of -0.75395% strain. The 3 gauges, which are only 75 μm apart, show a spread in strain values after the first -252 kN loading. Subsequently, due to the application and removal of the second 138 kN loading (which causes tensile yielding), the average strain is -0.16059% strain due to the residual compressive strain (cf 0.0.00552% strain after the first 138 kN loading). At the final part of the CPLT, a compressive loading to -252 kN causes material yielding again to occur in compression such that upon its removal there exists a residual compressive strain of -0.79349% strain. The strain results for gauge 7G at the sample flight loading of ±80 kN shows the continuing compressive residual strain effect of the CPLT. Here, a residual compressive strain of 0.51234% strain exists at the end of the sample loading. After the initial elastic response, all three gauges follow a consistent material hysteresis loop and show no significant indication of loop-to-loop drift.

5.2.2 Strains in area 3

The strain results for this area are summarised in Figure 10 (b) for each gauge, while Table 6 and Figure 11 give the average response for the gauges together. Strain hysteresis responses for three gauges during CPLT loading are given in Figures 16 to 18 respectively, while the corresponding area average strain response is given in Figure 19. Area 3 shows a similar strain response as area 1 during the CPLT as follows. There is an initial elastic response during the application and removal of the first tensile load of 138 kN. The subsequent high compressive loading to -252 kN and associated material yielding induces residual compressive strains which then have an effect on the remainder of the CPLT cycle. The residual compressive strain at the end of the CPLT loading is -0.37759% strain at 0 kN (cf -0.79349% strain for area 1). From Figures 10(a) and 10(b), it is seen that in contrast to area 1, the three gauges in area 3 show only a minimal variation in strain values at a specific load increment. This is to be expected due to the greater distance of area 3 from the hole edge and the associated reduction in local strain gradient. Also as expected, area 3 shows a lower compressive residual strain after the application of the -252 kN load and for the remainder of the CPLT cycle, as compared to area 1. It is interesting to note that gauge 4D shows some minor loop-to-loop drift but 1A and 7G show none, although it is not known why this effect has occurred. Also, the response of all three gauges indicate that the load-strain

hysteresis loop had not stabilised at the end of CPLT loading for area 3, in contrast to the situation for area 1.

5.2.3 Comparison with finite element results

In this report, a detailed comparison of the measured strain hysteresis responses, with those predicted by FE is not made. However it is useful to compare strain results at two key stages of the CPLT cycle. Firstly, at the first compressive peak load of -252kN, the microgrid result is -2.16024% strain in area 1, while the FE prediction is -2.1070% strain. Secondly, the measured residual strain after the CPLT cycle is completed is -0.79349% strain while the FE prediction is -0.8218% strain [4]. It can be seen that the agreement is very good. Furthermore, the detailed non-linear strain responses presented in the present work, provide useful benchmark data for validation of FE based constitutive modelling being currently undertaken in AED.

6. Conclusions

This report presents the development and application of an improved microgridding procedure for the determination of highly localised linear or non-linear strains. There are two contexts for the work, namely (i) F-111C airframe structural integrity, and (ii) improvements to the AED microgridding procedure for strain analysis of critical structural components.

6.1 F-111C Context

Testing of a microgridded specimen with elongated hole was successfully completed to determine plastic strains in the critical stress location representative of a reworked FFVH13. Here representative F-111C CPLT loading was applied to the plate as well as one cycle of a sample flight load. Multiple measurements of the microgrid were made over a 150 μm gauge length at various load points during the representative F-111C loading, to determine non linear strains. Highly accurate strains, ranging in accuracy between 57 and 135 micro strain were determined for these very-high-strain, low-cycle fatigue loading conditions. Two locations were analysed, and these were 0.137 and 2.208 mm respectively from the hole edge in the critical stress region. Detailed non linear strain hysteresis responses were obtained, and the measured peak and residual strains of -2.16024% strain and -0.79349% strain respectively, due to the CPLT, agreed well with prior strain gauge and FE work. As expected, the residual compressive strain is less for the location further from the hole edge. The residual compressive strains at the critical location indicate that there is a significant residual tensile stress, hence the reason for fatigue cracking in the fleet.

6.2 Improvements to microgridding method

The accuracy of the AED microgridding method has been improved by more than a factor of 10 as compared to previous work. Hence the method is now suitable for

determining highly accurate strain measurements under elastic or plasticity conditions, and its use is not restricted to the analysis of the very large distortion occurring at crack tips, as was previously the case. This has been achieved by the simple measures of increasing the gauge length to 150 μm and increasing the number of readings to 18. For high strain conditions, in particular fatigue loading, microgridding is now considered a much more accurate and reliable procedure than strain gauges. This is because of the well known degradation of the adhesive, (and hence strain readings) used to bond strain gauges for these conditions. For the same reasons, microgridding is particularly suited to stress relaxation and creep studies. One other useful feature is that the gauge length is about 4 times less than that for a typical small strain gauge, hence making it better able to capture strains where there is a significant strain gradient.

7. Acknowledgements

The authors wish to thank Mr R. Allan for his contributions to the experimental design, Mr N.R. Absolom for his technical support and Mr S.A. Barter for his assistance with specimen preparation. The authors also wish to acknowledge the helpful comments and suggestions provided by Mr K.C. Watters, Dr S. Pitt and Dr T.G. Ryall.

8. References

1 **KEYS, R.H., MOLENT, L. and GRAHAM, A.D.,** *F-111 wing pivot fitting finite element analysis of rework of fuel flow vent hole #13,* DSTO, ARL, Aircraft Structures Technical Memorandum 557, 1992.

2 **WATTERS, K.C.,** *Strain Surveys of Fuel Flow Vent Hole Number 13 and Stiffener Runout Number 2 in the F-111 Wing Pivot Fitting for a Range of Rework Shapes,* DSTO, AMRL, Technical Report, DSTO-TR-0567, August 1997.

3 **PAUL, J.J., CHAPMAN, P. and SEARL, A.,** *Elastic/Plastic finite element analysis of the F-111 fuel flow vent hole number 13,* DSTO, AMRL Technical Report No. 454, November 1996.

4 **ALLAN, R.,** *Elastic - Plastic Stress Analysis of a Plate with a Central Elongated Hole - Comparison of Experiment with Finite Element Analysis Containing the Unified Constitutive Material Model,* AMRL File M1/9/395.

5 **SEARL, A. and PAUL, J.J.,** *Characterisation of D6AC Steel Using A Unified Constitutive Model,* DSTO, AMRL Technical Report No. 556, July 1997.

6 **BEAVER, P.,** *An Evaluation of Microgridding Techniques for determining Local Plastic Strain Distributions,* DSTO, ARL, Structures Technical Memorandum 454, 1986.

7 **BEAVER, P., MANN, J.Y. and SPARROW, J.G.,** *A grid technique for the measurement of strains close to cold-expanded holes,* Measurement and Fatigue -- EIS-86, 1986.

8 **HELLER, M., JONES, R. and WILLIAMS, J.F.,** *Analysis of Cold-Expansion for Cracked and Uncracked Fastener Holes,* Engineering Fracture Mechanics, Vol. 39, No. 2, pp 195-212, 1991.

9 **HOLMAN, J. P. and GAJDA, W.J.** *Experimental Methods for Engineers,* 4th edition, published by McGraw-Hill, 1984.

10 **ALLAN, R. A. and HELLER,** *Stress analysis of an interference fit life extension option for a cold expanded elongated fuel flow vent hole on the F-111C aircraft,* DSTO, AMRL Technical Report, DSTO-TR-0549, June 1997.

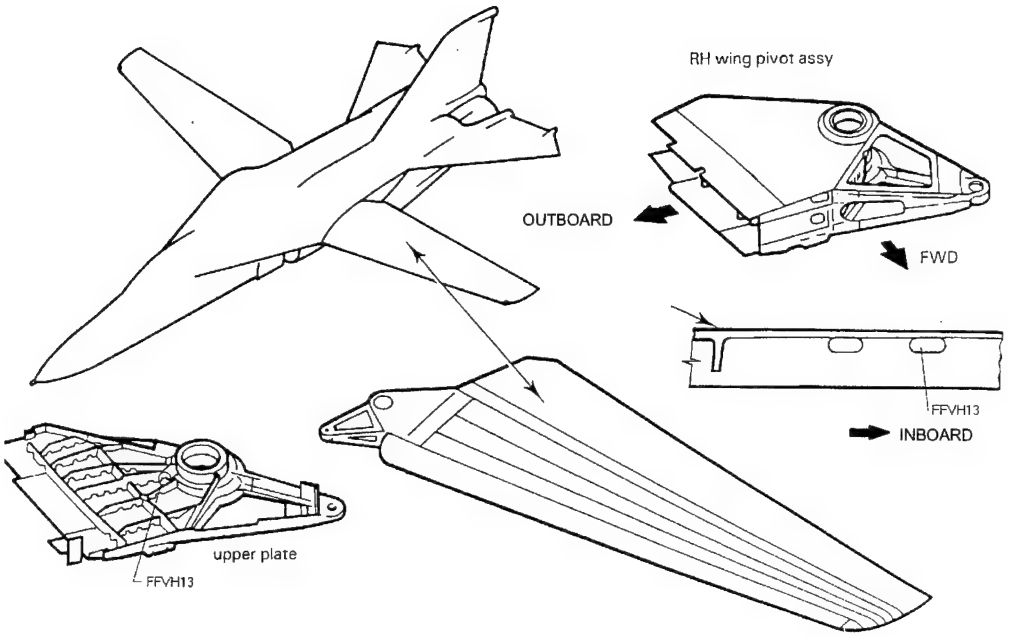

Figure 1. F-111C Aircraft and wing, showing location of fuel flow vent hole number 13 (FFVH13) in the wing pivot fitting.

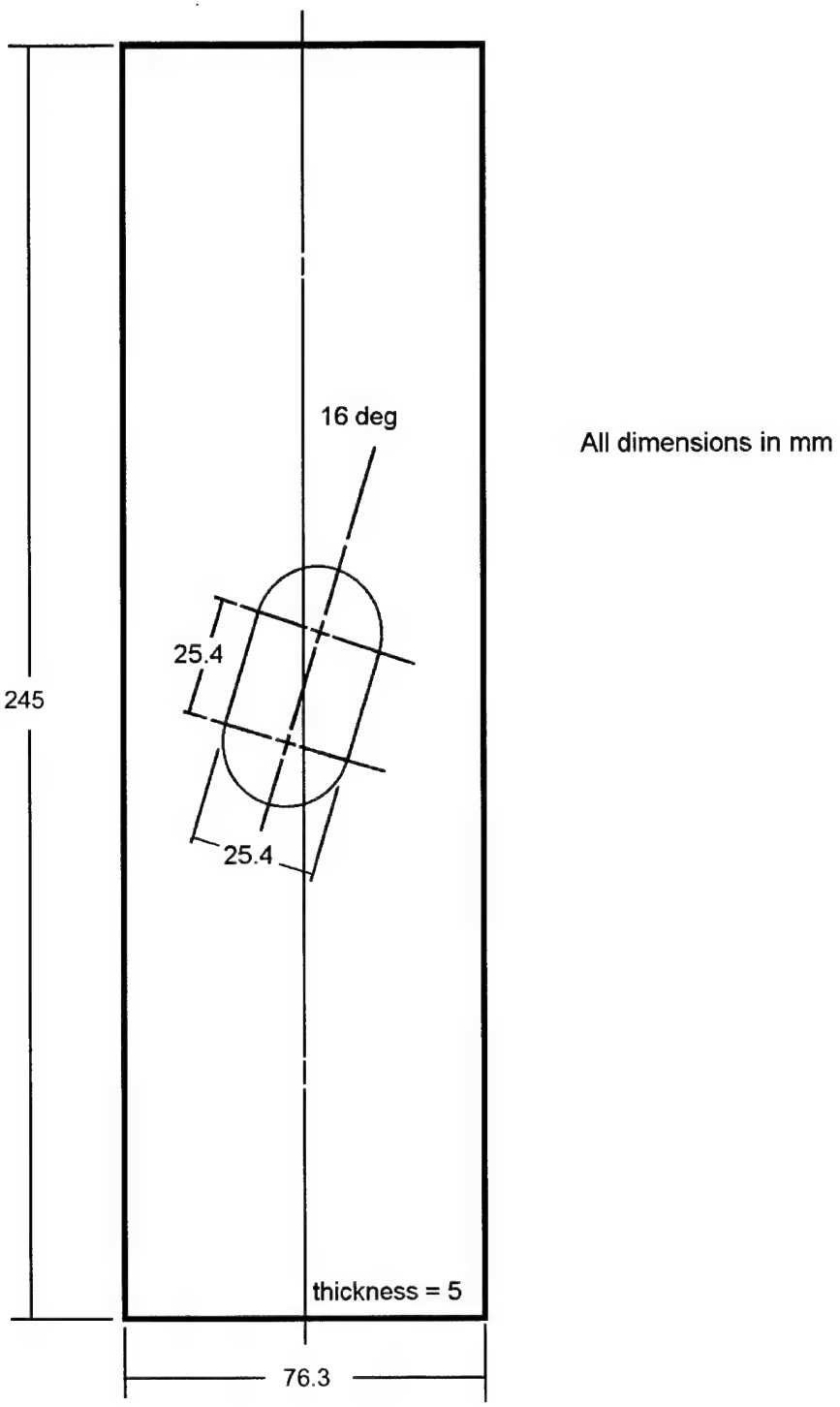

Figure 2. Geometry of plate specimen representative of an oversized fuel flow vent hole 13.

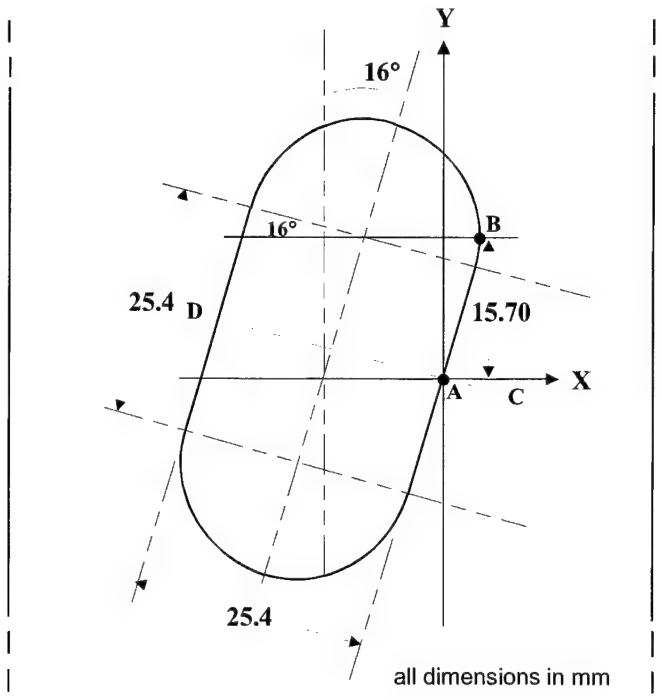

Figure 3. Location of critical stress area (point B) on the specimen with reference to the coordinate origin (point A).

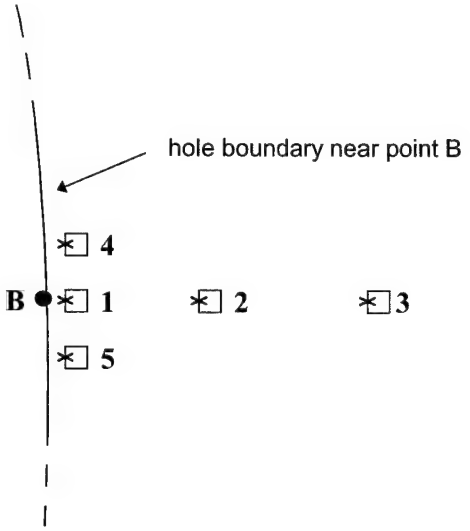

Figure 4. Enlargement of critical stress location (Point B, Fig 3) showing the 5 measurement areas (each consisting of a 7 x 7 grid). The point "X" marked on each area is located in the specimen X-Y axis system as given in Table 1.

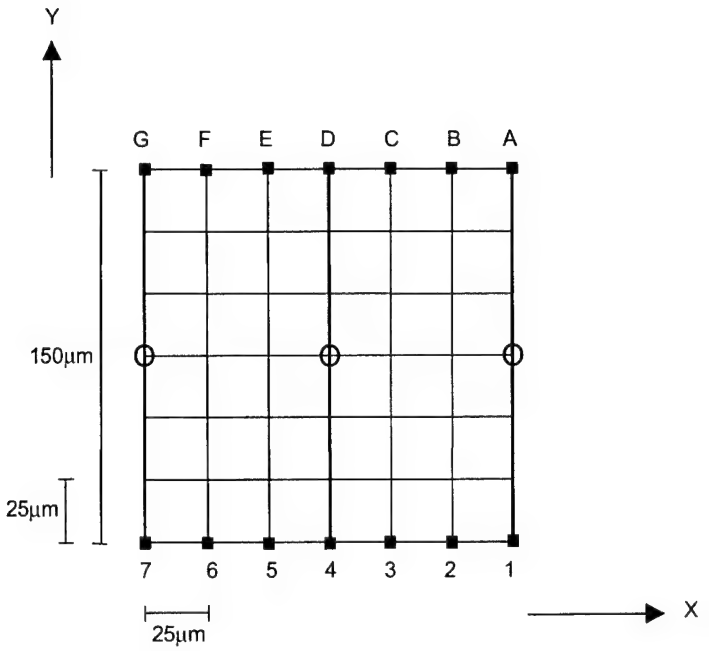

Figure 5. Location of the three gauges (1A, 4D and 7G) each of 150μm length on a typical measurement area consisting of a 7 x 7 grid. The mid-point (symbol O) on each 150μm gauge length represents the location with reference to the specimen X-Y system having the origin at point A (Figure 3).

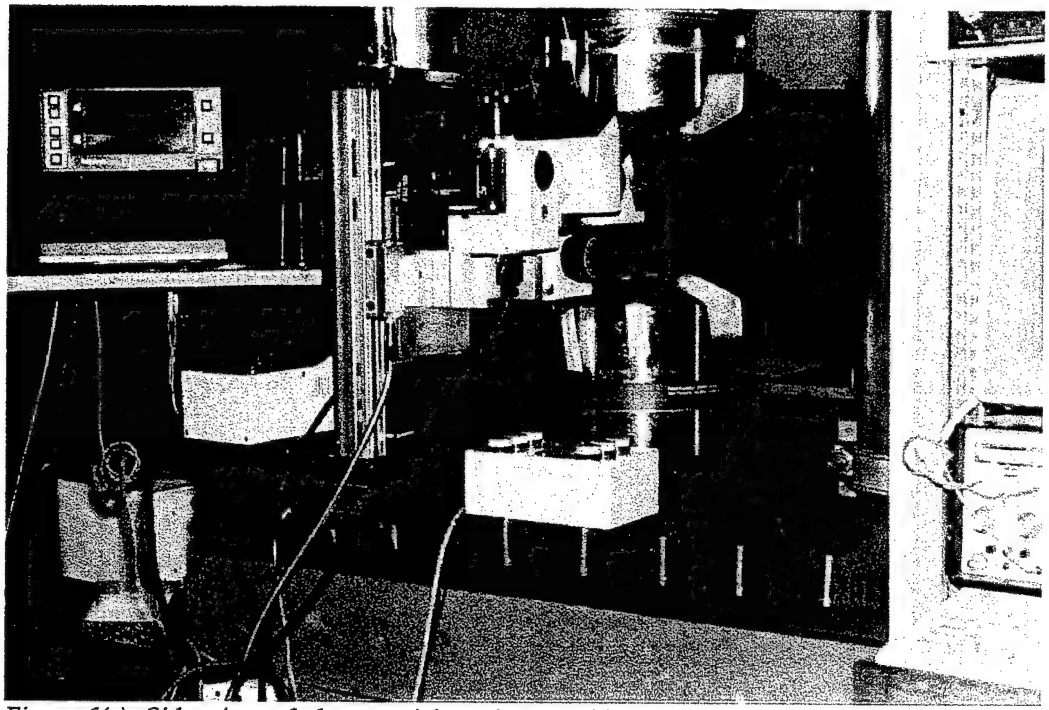

Figure 6(a). Side view of the unaxial testing machine and the photographic system with positioning equipment.

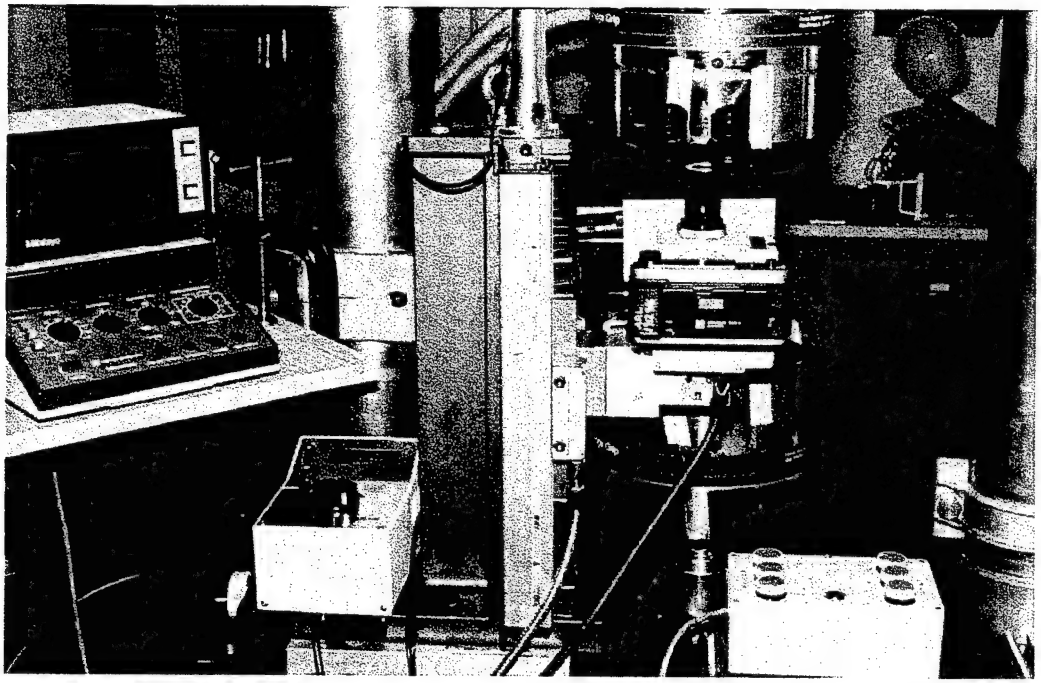

Figure 6(b). Equipment used for the positioning and photographic recording of the 5 measurement areas (each consisting of a 7 x 7 grid) during loading. Shown is the X-Z traversing stage and the microscope arrangement.

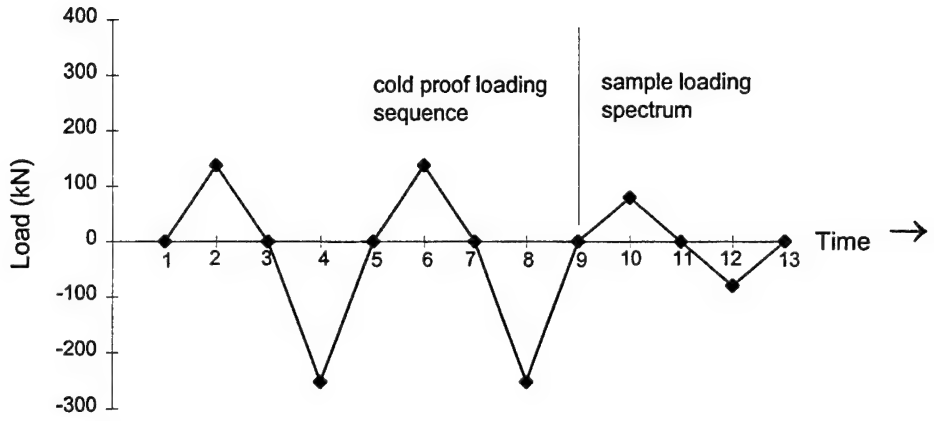

Figure 7. Sequence of load points on CPLT and sample loading spectrum

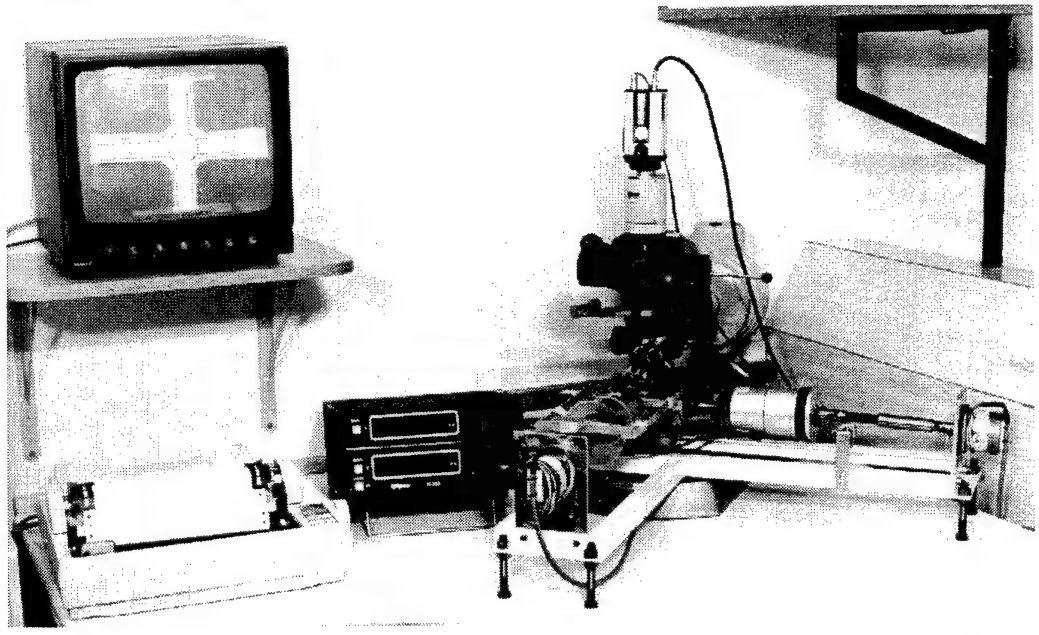

Figure 8. Instrumentation for enlargement of the 35mm negative and subsequent measurement of grid point displacements.

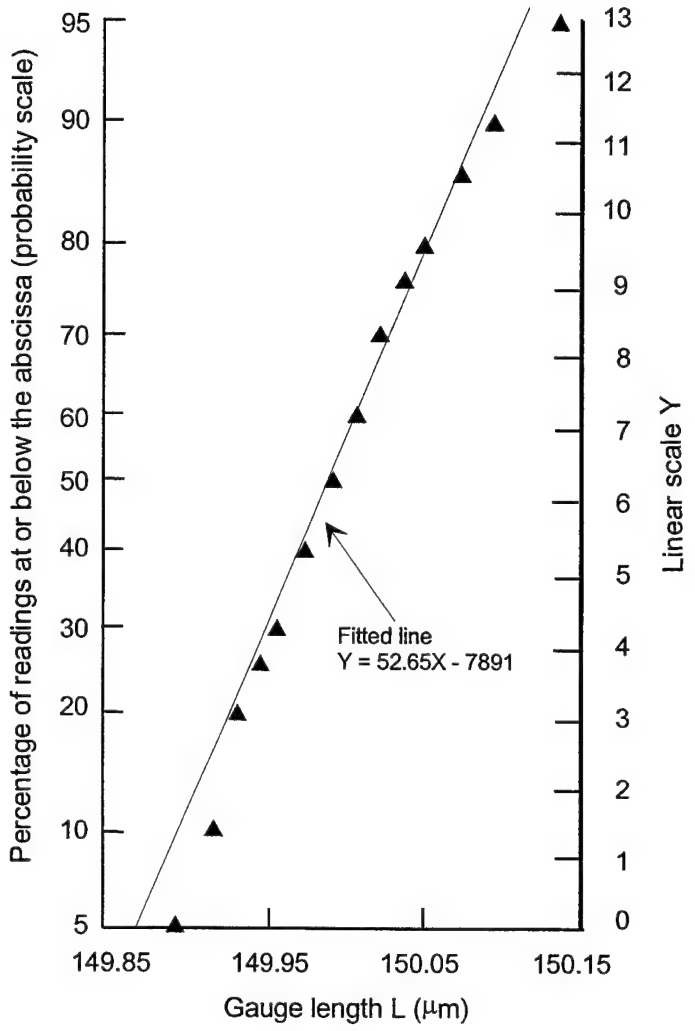

Figure 9. Graphical assessment of normality of data distribution for the 18 gauge length measurements of gauge 7G in area 1 at load point 1 (ie 0kN).

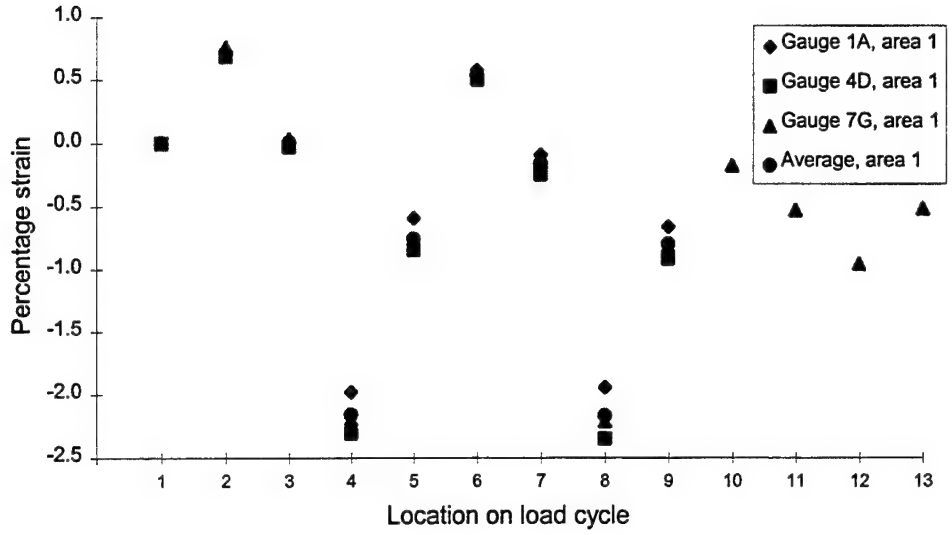

Figure 10(a). Strain response for area 1 during CPLT and sample loading.

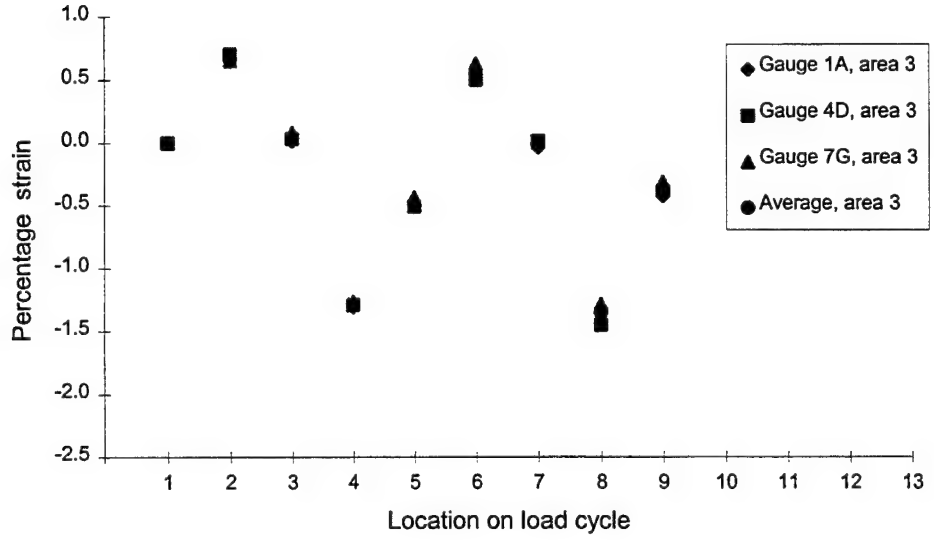

Figure 10(b). Strain response for area 3 during CPLT.

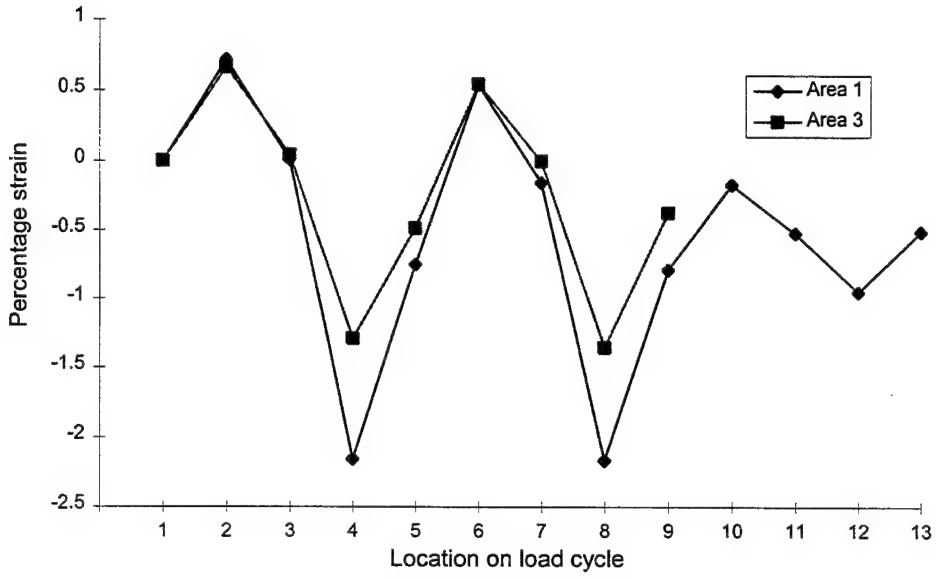

Figure 11. Strain response (average of 3 gauge lengths) for areas 1 and 3 during CPLT

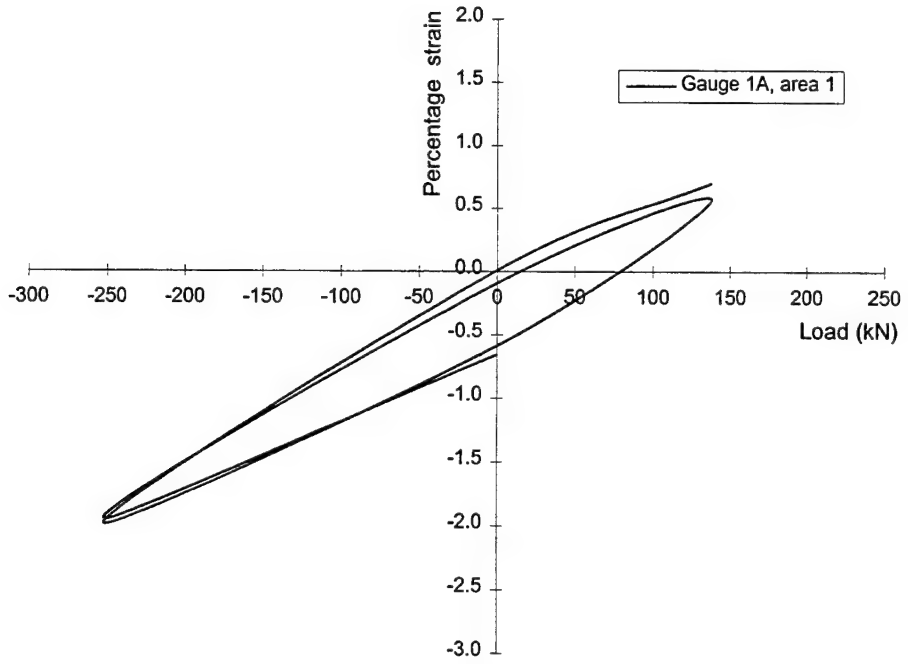

Figure 12. Strain hysteresis response for gauge 1A in area 1 during CPLT loading.

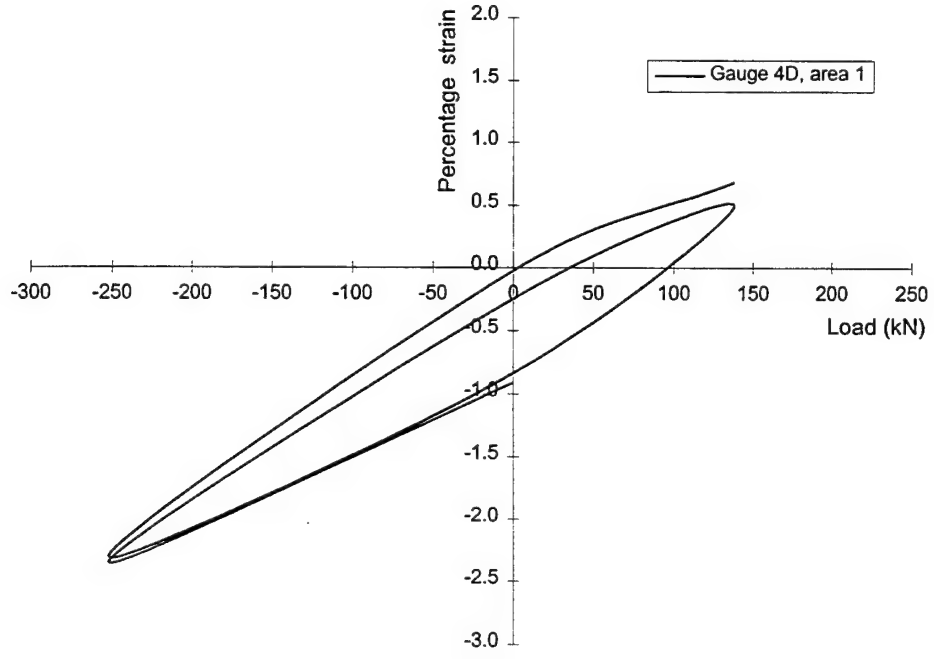

Figure 13. Strain hysteresis response for gauge 4D in area 1 during CPLT loading.

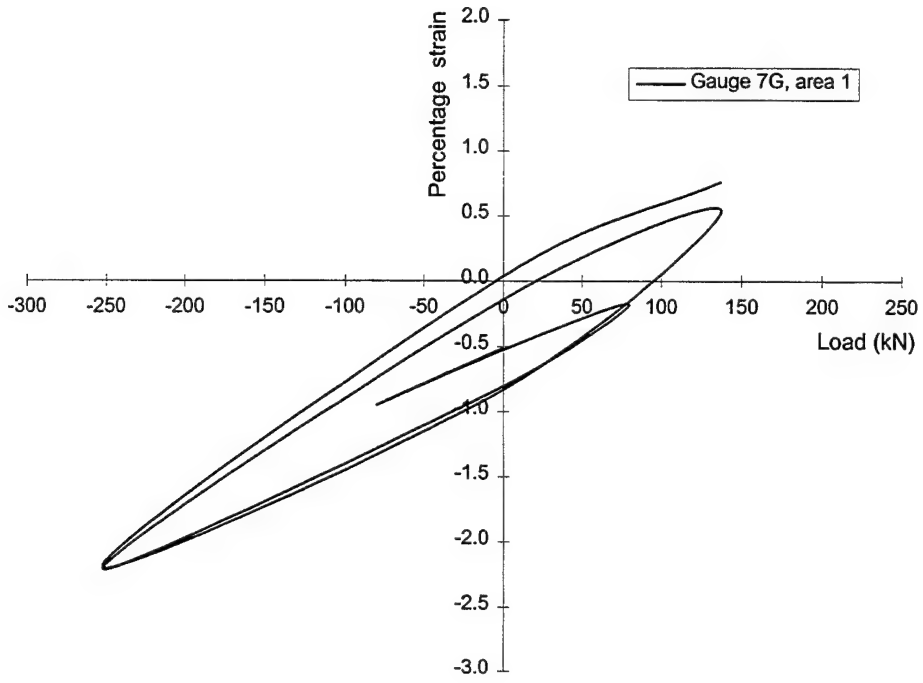

Figure 14. Strain hysteresis response for gauge 7G in area 1 during CPLT and sample

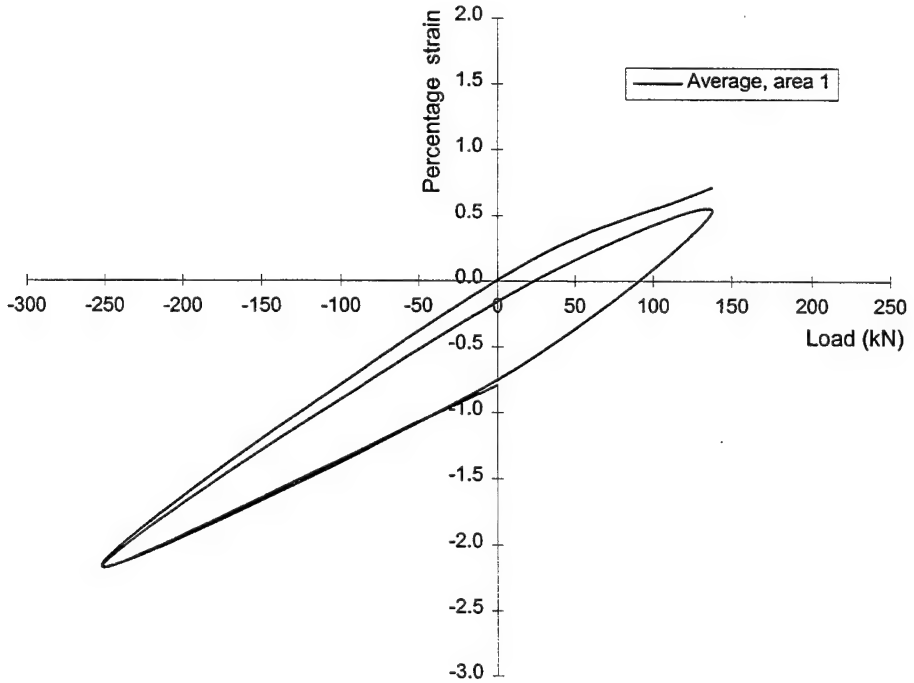

Figure 15. Strain hysteresis response for the average of three gauges (1A, 4D and 7G)

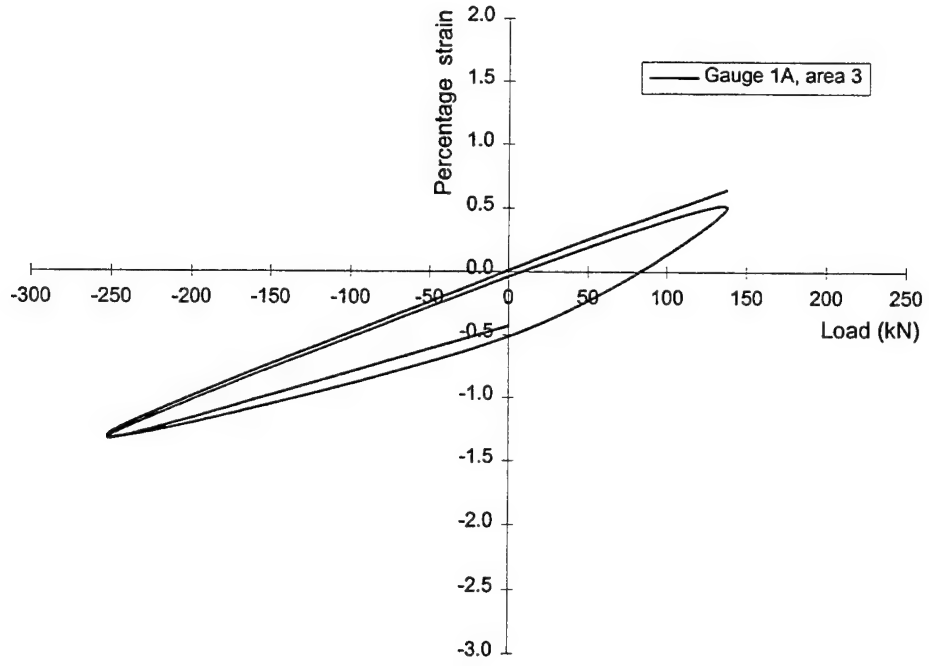

Figure 16. Strain hysteresis response for gauge 1A in area 3 during CPLT loading.

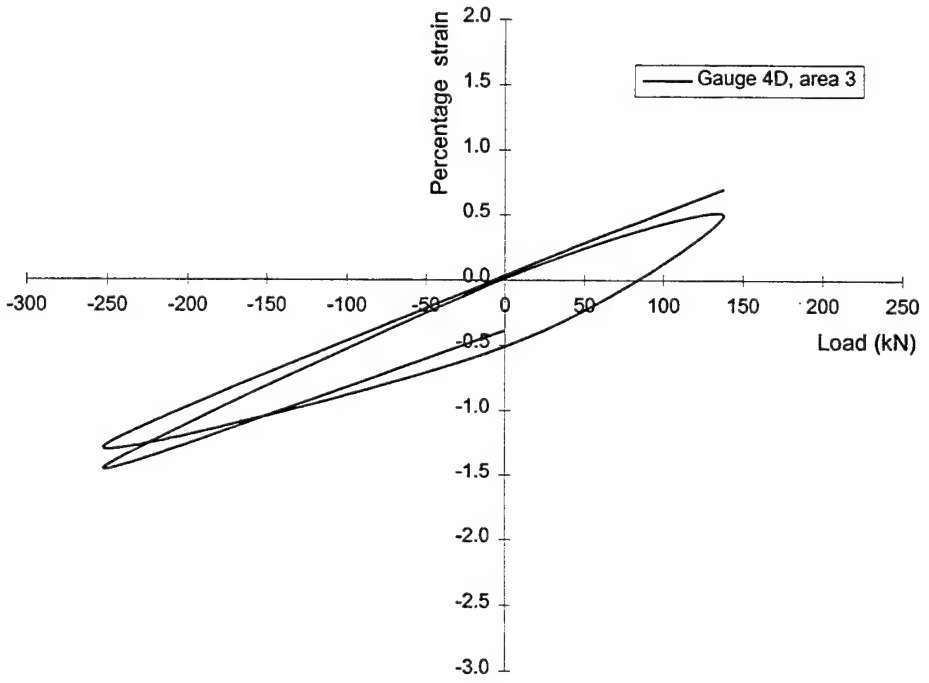

Figure 17. Strain hysteresis response for gauge 4D in area 3 during CPLT loading.

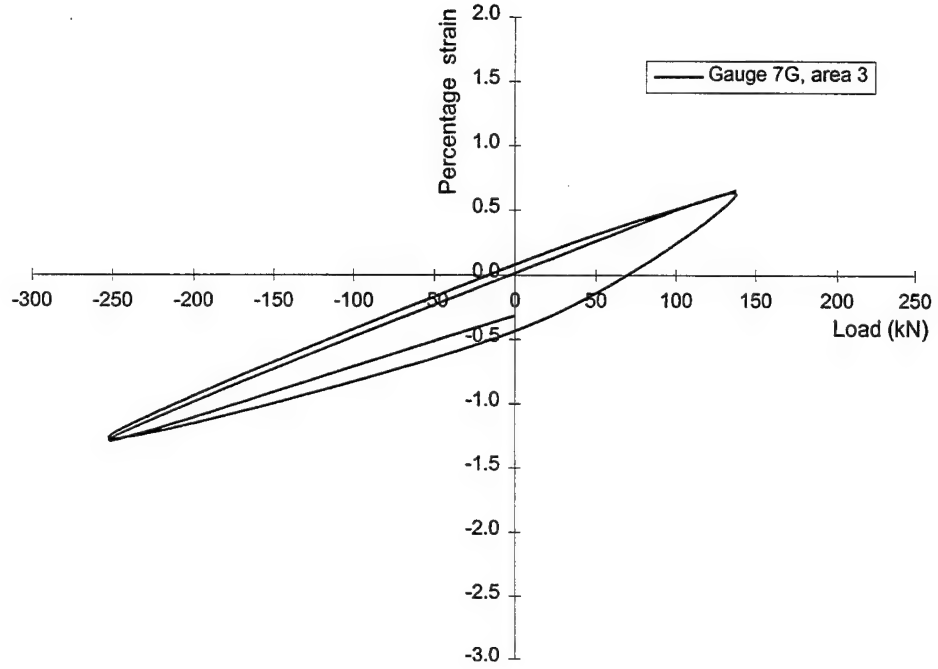

Figure 18. Strain hysteresis response for gauge 7G in area 3 during CPLT loading.

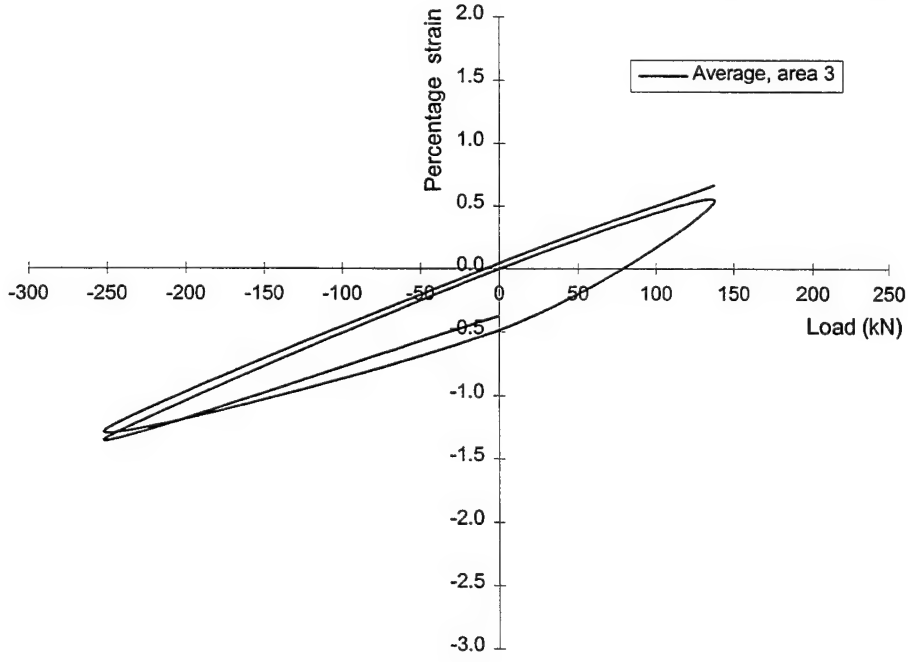

Figure 19. Strain hysteresis response for the average of three gauges (1A, 4D and 7G)

Table 1: Location in the X-Y coordinate system of the centre of the first gauge (point X, Figure 4) in each of the 5 measurements areas (each consisting of a 7 x 7 grid) at the critical stress location (point B, Figure 3) at zero load calibration.

Area	X coordinate (mm)	Y coordinate (mm)	Distance from edge of hole, X direction (mm)
1	4.097	15.691	0.137
2	5.360	15.714	1.400
3	6.168	15.725	2.208
4	4.092	16.743	-
5	5.110	14.727	-

Table 2: Location in the X-Y coordinate system of the centre of the three 150 μm gauge lengths (symbol O, Figure 5) within the five measurement areas (each consisting of a 7 x 7 grid).

Area	Gauge	X coordinate (mm)	Y coordinate (mm)	Distance from edge of hole, X direction (mm)
1	7G	4.097	15.691	0.137
1	4D	4.172	15.691	0.212
1	1A	4.247	15.691	0.287
2	7G	5.360	15.714	1.400
2	4D	5.435	15.714	1.475
2	1A	5.510	15.714	1.550
3	7G	6.168	15.725	2.208
3	4D	6.243	15.725	2.283
3	1A	6.318	15.725	2.358
4	7G	4.092	16.743	-
4	4D	4.167	16.743	-
4	1A	4.167	16.743	-
5	7G	5.110	14.727	-
5	4D	5.185	14.727	-
5	1A	5.260	14.727	-

Table 3 : Analysis results for gauge lengths in area 1 for 18 measurements.

Location on load cycle	Load (kN)	Gauge 1A				Gauge 4D				Gauge 7G			
		Average length ($\bar{L}$) (µm)	Average strain ($\bar{\varepsilon}$) (%strain)	Standard deviation of strain ($\sigma\varepsilon$) (%strain)	Accuracy of strain $\left(\frac{\sigma\varepsilon}{\sqrt{n}}\right)$ (%strain)	Average length ($\bar{L}$) (µm)	Average strain ($\bar{\varepsilon}$) (%strain)	Standard deviation of strain ($\sigma\varepsilon$) (%strain)	Accuracy of strain $\left(\frac{\sigma\varepsilon}{\sqrt{n}}\right)$ (%strain)	Average length ($\bar{L}$) (µm)	Average strain ($\bar{\varepsilon}$) (%strain)	Standard deviation of strain ($\sigma\varepsilon$) (%strain)	Accuracy of strain $\left(\frac{\sigma\varepsilon}{\sqrt{n}}\right)$ (%strain)
1	0	150.0000	0.0000	0.0534	0.0125	149.9999	0.0000	0.0435	0.0102	149.9999	0.0000	0.0360	0.0085
2	138	151.0545	0.7030	0.0399	0.0094	151.0222	0.6815	0.0504	0.0118	151.1407	0.7604	0.0285	0.0067
3	0	150.0124	0.0082	0.0573	0.0135	149.9591	-0.0272	0.0588	0.0138	150.0532	0.0355	0.0427	0.0100
4	-252	147.0262	-1.9825	0.0327	0.0077	146.5413	-2.3058	0.0369	0.0087	146.7113	-2.1924	0.0329	0.0077
5	0	149.1156	-0.5895	0.0327	0.0077	148.7420	-0.8398	0.0348	0.0082	148.7512	-0.8325	0.0460	0.0108
6	138	150.8631	0.5754	0.0403	0.0095	150.7492	0.4995	0.0499	0.0117	150.8071	0.5381	0.0412	0.0097
7	0	149.8611	-0.0925	0.0470	0.0110	149.6300	-0.2466	0.0383	0.0097	149.7861	-0.1425	0.0383	0.0090
8	-252	147.0839	-1.9440	0.0461	0.0108	146.4756	-2.3495	0.0360	0.0085	146.6821	-2.2118	0.0350	0.0082
9	0	149.0119	-0.6587	0.0356	0.0083	148.6289	-0.9140	0.0320	0.0079	148.7884	-0.8076	0.0333	0.0078
10	80	-	-	-	-	-	-	-	-	149.7358	-0.1761	0.0400	0.0094
11	0	-	-	-	-	-	-	-	-	149.2110	-0.5259	0.0376	0.0088
12	-80	-	-	-	-	-	-	-	-	148.5688	-0.9541	0.0409	0.0096
13	0	-	-	-	-	-	-	-	-	149.2314	-0.5123	0.0376	0.0088

Table 4 : Analysis results for gauge lengths in area 3 for 18 measurements.

Location on load cycle	Load (kN)	Gauge 1A				Gauge 4D				Gauge 7G			
		Average length ($\bar{L}$) (μm)	Average strain ($\bar{\varepsilon}$) (%strain)	Standard deviation of strain ($\sigma\varepsilon$) (%strain)	Accuracy of strain $\left(\frac{\sigma\varepsilon}{\sqrt{n}}\right)$ (%strain)	Average length ($\bar{L}$) (μm)	Average strain ($\bar{\varepsilon}$) (%strain)	Standard deviation of strain ($\sigma\varepsilon$) (%strain)	Accuracy of strain $\left(\frac{\sigma\varepsilon}{\sqrt{n}}\right)$ (%strain)	Average length ($\bar{L}$) (μm)	Average strain ($\bar{\varepsilon}$) (%strain)	Standard deviation of strain ($\sigma\varepsilon$) (%strain)	Accuracy of strain $\left(\frac{\sigma\varepsilon}{\sqrt{n}}\right)$ (%strain)
1	0	149.9999	0.0000	0.0452	0.0106	149.9999	0.0000	0.0423	0.0099	149.9999	0.0000	0.0453	0.0106
2	138	150.9746	0.6458	0.0357	0.0084	151.0356	0.7006	0.0426	0.0100	150.9782	0.6526	0.0471	0.0111
3	0	149.9853	0.0097	0.0482	0.0113	150.0467	0.0311	0.0516	0.0105	150.1205	0.0803	0.0343	0.0081
4	-252	148.0332	-1.3111	0.0384	0.0090	148.0595	-1.2936	0.0299	0.0073	148.0989	-1.2673	0.0255	0.0060
5	0	149.2284	-0.5143	0.0312	0.0073	149.2339	-0.5107	0.0387	0.0074	149.3439	-0.4373	0.0243	0.0057
6	138	150.7576	0.5050	0.0425	0.0100	150.7471	0.4980	0.0440	0.0102	150.9366	0.6244	0.0432	0.0102
7	0	149.9386	-0.0409	0.0401	0.0094	150.0160	0.0107	0.0387	0.0091	150.0219	0.0146	0.0338	0.0079
8	-252	148.0105	-1.3262	0.0467	0.0110	147.8207	-1.4528	0.0419	0.0099	148.0675	-1.2883	0.0497	0.0117
9	0	149.3556	-0.4296	0.0418	0.0098	149.4194	-0.3870	0.0358	0.0084	149.5248	-0.3161	0.0375	0.0088

Table 5 : Calculated percentage strain for gauge lengths in area 1

Location on load cycle	Load (kN)	Calculated percentage strain			
		Gauge 1A	Gauge 4D	Gauge 7G	Average
1	0	0.00000	0.00001	0.00001	0.00001
2	138	0.70306	0.68152	0.76048	0.71502
3	0	0.00828	-0.02725	0.03551	0.00552
4	-252	-1.98251	-2.30580	-2.19242	-2.16024
5	0	-0.58954	-0.83982	-0.83250	-0.75395
6	138	0.57541	0.49951	0.53813	0.53768
7	0	-0.09257	-0.24663	-0.14257	-0.16059
8	-252	-1.94402	-2.34958	-2.21188	-2.16849
9	0	-0.65873	-0.91405	-0.80769	-0.79349
10	80	-	-	-0.17614	-
11	0	-	-	-0.52596	-
12	-80	-	-	-0.95413	-
13	0	-	-	-0.51234	-

Table 6 : Calculated percentage strain for gauge lengths in area 3

Location on load cycle	Load (kN)	Calculated percentage strain			
		Gauge 1A	Gauge 4D	Gauge 7G	Average
1	0	0.00001	0.00001	0.00001	0.00001
2	138	0.64585	0.70063	0.65267	0.66638
3	0	0.00975	0.03117	0.08036	0.04042
4	-252	-1.31119	-1.29365	-1.26735	-1.29073
5	0	-0.51435	-0.51074	-0.43739	-0.48749
6	138	0.50509	0.49809	0.62442	0.54253
7	0	-0.04092	0.01072	0.01461	-0.00520
8	-252	-1.32629	-1.45286	-1.28830	-1.35582
9	0	-0.42960	-0.38707	-0.31611	-0.37759

Appendix A

Raw experimental results for gauges in area 1

Table A.1. Results for gauge length measurements at load 1 (0 kN calibration)

Reading	Length of nominal 150 μm gauges (μm)		
	Gauge 1A	Gauge 4D	Gauge 7G
1	149.92765	149.94089	150.02408
2	149.84872	149.99343	149.93212
3	150.07235	150.09851	149.95840
4	149.98027	149.92776	149.93212
5	150.00658	150.01970	149.98467
6	150.09866	150.01970	149.94526
7	149.87503	149.91463	149.98467
8	149.96711	150.11164	150.08977
9	149.92765	150.01970	150.08977
10	150.01973	149.99343	150.01095
11	150.00658	150.03283	150.07663
12	149.96711	150.01970	150.02408
13	150.12497	150.09851	149.97154
14	150.13813	149.91463	149.99781
15	150.00658	149.98030	149.91899
16	149.95396	149.91463	150.05036
17	150.07235	149.94089	150.03722
18	150.00658	150.05910	149.97154
19	149.84872	149.90149	150.12918
20	150.15128	150.13791	149.89271

Table A.2. Results for gauge length measurements at load 2 (138 kN)

Reading	Length of nominal 150 μm gauges (μm)		
	Gauge 1A	Gauge 4D	Gauge 7G
1	151.11160	151.00477	151.10131
2	151.04582	151.04417	151.12759
3	151.07213	150.93910	151.11445
4	151.12475	151.00477	151.14072
5	151.09844	150.91283	151.19327
6	151.11160	151.00477	151.07504
7	151.07213	151.09671	151.10131
8	151.05898	151.05731	151.14072
9	151.05898	150.95223	151.19327
10	150.88796	151.00477	151.15386
11	151.03267	151.09671	151.08818
12	151.03267	150.97850	151.16700
13	151.00636	151.14925	151.14072
14	151.07213	150.96537	151.15386
15	151.12475	151.18865	151.12759
16	150.95374	151.01791	151.20641
17	151.07213	150.92597	151.08818
18	151.04582	151.05731	151.21955
19	151.11160	151.20179	151.24582
20	150.98005	151.18865	151.03563

Table A.3. Results for gauge length measurements at load 3 (0 kN)

Reading	Length of nominal 150 μm gauges (μm)		
	Gauge 1A	Gauge 4D	Gauge 7G
1	149.99342	150.09851	150.05036
2	150.12497	149.99343	150.05036
3	149.91449	149.98030	149.91899
4	150.13813	149.83582	149.99781
5	149.88818	150.04597	150.11604
6	149.92765	149.80955	150.12918
7	149.99342	150.05910	150.14232
8	149.95396	149.84895	150.14232
9	150.00658	149.92776	150.10290
10	149.91449	149.99343	150.03722
11	149.98027	150.05910	150.06349
12	150.05920	149.92776	150.10290
13	150.08551	149.91463	149.95840
14	150.11182	149.83582	150.07663
15	150.07235	150.07224	150.02408
16	150.15128	149.94089	150.05036
17	149.91449	149.94089	150.02408
18	149.99342	149.98030	149.97154
19	149.84872	150.11164	149.91899
20	150.17759	149.78328	150.16859

Table A.4. Results for gauge length measurements at load 4 (-252 kN)

Reading	Length of nominal 150 μm gauges (μm)		
	Gauge 1A	Gauge 4D	Gauge 7G
1	146.98093	146.60479	146.77925
2	146.95462	146.55225	146.75298
3	146.96777	146.42091	146.66102
4	147.07301	146.52598	146.63475
5	147.04670	146.63106	146.72671
6	147.00724	146.56539	146.71357
7	147.03355	146.55225	146.64788
8	146.98093	146.56539	146.75298
9	147.00724	146.44718	146.75298
10	146.95462	146.53912	146.63475
11	147.09932	146.59165	146.75298
12	146.99408	146.51285	146.66102
13	147.04670	146.49971	146.76612
14	147.07301	146.49971	146.72671
15	147.02039	146.53912	146.66102
16	147.03355	146.60479	146.70043
17	147.09932	146.49971	146.71357
18	147.09932	146.59165	146.76612
19	147.16510	146.47345	146.79239
20	147.12563	146.47345	146.63475

Table A.5. Results for gauge length measurements at load 5 (0 kN)

Reading	Length of nominal 150 μm gauges (μm)		
	Gauge 1A	Gauge 4D	Gauge 7G
1	149.13835	148.70627	148.68411
2	149.08573	148.69314	148.86803
3	149.15150	148.70627	148.72352
4	149.19097	148.69314	148.89430
5	149.04626	148.75881	148.68411
6	149.15150	148.79821	148.71039
7	149.08573	148.79821	148.71039
8	149.13835	148.77194	148.74980
9	149.09888	148.69314	148.68411
10	149.07257	148.66687	148.88117
11	149.13835	148.79821	148.77607
12	149.04626	148.75881	148.73666
13	149.08573	148.70627	148.68411
14	149.07257	148.71941	148.73666
15	149.19097	148.86388	148.77607
16	149.13835	148.69314	148.69725
17	149.19097	148.75881	148.80235
18	149.05942	148.77194	148.72352
19	149.12519	148.83762	148.44765
20	149.16466	148.69314	148.80235

Table A.6. Results for gauge length measurements at load 6 (138 kN)

Reading	Length of nominal 150 μm gauges (μm)		
	Gauge 1A	Gauge 4D	Gauge 7G
1	150.82219	150.76752	150.85171
2	150.96689	150.67555	150.83857
3	150.90112	150.74124	150.81230
4	150.94058	150.88576	150.87799
5	150.79588	150.64928	150.90426
6	150.92743	150.72810	150.73348
7	150.83534	150.84634	150.85171
8	150.91427	150.70183	150.73348
9	150.91427	150.71497	150.77289
10	150.76957	150.83321	150.73348
11	150.82219	150.70183	150.86485
12	150.82219	150.88576	150.85171
13	150.92743	150.71497	150.69407
14	150.83534	150.70183	150.79916
15	150.84850	150.66242	150.72034
16	150.79588	150.72810	150.81230
17	150.79588	150.83321	150.82544
18	150.90112	150.71497	150.85171
19	150.98005	150.92517	150.96994
20	150.76957	150.63614	150.95681

Table A.7. Results for gauge length measurements at load 7 (0 kN)

Reading	Length of nominal 150 μm gauges (μm)		
	Gauge 1A	Gauge 4D	Gauge 7G
1	149.79610	149.67821	149.76134
2	149.78294	149.58627	149.80075
3	149.94080	149.70448	149.70880
4	149.88818	149.70448	149.78762
5	149.91449	149.61254	149.68252
6	149.79610	149.59940	149.74821
7	149.94080	149.74388	149.81389
8	149.83556	149.54687	149.81389
9	149.78294	149.66508	149.87958
10	149.80925	149.58627	149.73507
11	149.92765	149.58627	149.73507
12	149.78294	149.63881	149.72193
13	149.79610	149.57314	149.84017
14	149.80925	149.57314	149.78762
15	149.96711	149.65194	149.84017
16	149.95396	149.56000	149.84017
17	149.83556	149.65194	149.87958
18	149.94080	149.67821	149.77448
19	149.98027	149.54687	149.62997
20	149.98027	149.79642	149.87958

Table A.8. Results for gauge length measurements at load 8 (-252 kN)

Reading	Length of nominal 150 μm gauges (μm)		
	Gauge 1A	Gauge 4D	Gauge 7G
1	147.13879	146.52598	146.68730
2	146.98093	146.46031	146.73984
3	147.03355	146.51285	146.70043
4	147.16510	146.43404	146.71357
5	147.15194	146.48658	146.64788
6	147.13879	146.38151	146.67416
7	147.19141	146.40777	146.64788
8	147.00724	146.53912	146.67416
9	147.13879	146.51285	146.64788
10	147.02039	146.49971	146.62161
11	147.09932	146.39464	146.62161
12	147.07301	146.38151	146.59534
13	147.19141	146.53912	146.76612
14	147.03355	146.48658	146.76612
15	147.07301	146.48658	146.63475
16	146.99408	146.47345	146.66102
17	147.03355	146.49971	146.72671
18	147.04670	146.53912	146.75298
19	147.00724	146.32897	146.56906
20	147.15194	146.34210	146.77925

Table A.9. Results for gauge length measurements at load 9 (0 kN)

Reading	Length of nominal 150 μm gauges (μm)		
	Gauge 1A	Gauge 4D	Gauge 7G
1	148.99364	148.68000	148.80235
2	149.08573	148.56180	148.72352
3	149.05942	148.68000	148.80235
4	149.00680	148.60120	148.81548
5	148.95418	148.66687	148.84176
6	148.94102	148.62747	148.72352
7	149.07257	148.62747	148.84176
8	149.09888	148.56180	148.82862
9	149.05942	148.61433	148.81548
10	148.96733	148.64060	148.73666
11	148.94102	148.71941	148.73666
12	149.05942	148.57493	148.71039
13	149.07257	148.70627	148.80235
14	148.99364	148.56180	148.84176
15	148.98049	148.62747	148.84176
16	148.99364	148.64060	148.78921
17	148.96733	148.60120	148.71039
18	148.96733	148.62747	148.82862
19	148.91471	148.74568	148.90744
20	149.09888	148.71941	148.69725

Table A.10. Results for gauge length measurements at load 10 (80 kN)

Reading	Length of nominal 150 μm gauges (μm)
	Gauge 4D
1	149.72193
2	149.80075
3	149.66939
4	149.72193
5	149.77448
6	149.73507
7	149.65625
8	149.84017
9	149.68252
10	149.72193
11	149.68252
12	149.64311
13	149.70880
14	149.82703
15	149.78762
16	149.77448
17	149.69566
18	149.80075
19	149.61684
20	149.61684

Table A.11. Results for gauge length measurements at load 11 (0 kN)

Reading	Length of nominal 150 μm gauges (μm)
	Gauge 4D
1	149.24900
2	149.13077
3	149.19645
4	149.18332
5	149.24900
6	149.15704
7	149.11763
8	149.27528
9	149.23587
10	149.22273
11	149.19645
12	149.22273
13	149.13077
14	149.20959
15	149.22273
16	149.32782
17	149.28841
18	149.18332
19	149.28841
20	149.35410

Table A.12. Results for gauge length measurements at load 12 (-80 kN)

Reading	Length of nominal 150 μm gauges (μm)
	Gauge 4D
1	148.48706
2	148.44765
3	148.63157
4	148.60529
5	148.63157
6	148.52647
7	148.63157
8	148.55274
9	148.64470
10	148.57902
11	148.60529
12	148.57902
13	148.64470
14	148.56588
15	148.51333
16	148.52647
17	148.59215
18	148.47392
19	148.65784
20	148.39510

Table A.13. Results for gauge length measurements at load 13 (0 kN)

Reading	Length of nominal 150 μm gauges (μm)
	Gauge 4D
1	149.27528
2	149.26214
3	149.23587
4	149.11763
5	149.14391
6	149.23587
7	149.26214
8	149.28841
9	149.26214
10	149.26214
11	149.20959
12	149.30155
13	149.15704
14	149.24900
15	149.30155
16	149.24900
17	149.14391
18	149.20959
19	149.09136
20	149.10450

Appendix B

Raw experimental results for gauges in area 3

Table B.1. Results for gauge length measurements at load 1 (0 kN calibration)

Reading	Length of nominal 150 μm gauges (μm)		
	Gauge 1A	Gauge 4D	Gauge 7G
1	149.91963	149.98176	149.90648
2	150.03799	149.95546	150.01169
3	150.03799	150.08692	149.91963
4	150.02484	149.92917	149.94593
5	149.99854	149.99490	149.97224
6	150.11690	149.92917	149.93278
7	149.89333	150.00805	150.05114
8	150.02484	150.10007	150.09059
9	149.95909	149.92917	149.99854
10	150.06429	149.91603	150.09059
11	150.07744	149.96861	150.03799
12	150.05114	149.96861	149.90648
13	149.99854	150.08692	150.09059
14	149.93278	150.08692	149.91963
15	150.01169	150.08692	150.01169
16	149.88018	150.02119	150.06429
17	150.05114	149.98176	149.97224
18	149.91963	149.96861	150.07744
19	150.10374	149.94232	149.90648
20	149.89333	149.91603	150.09059

Table B.2. Results for gauge length measurements at load 2 (138 kN)

Reading	Length of nominal 150 μm gauges (μm)		
	Gauge 1A	Gauge 4D	Gauge 7G
1	151.03745	151.04657	150.93225
2	150.93225	151.12545	151.02430
3	151.02430	150.98085	150.97170
4	151.05061	150.98085	151.01115
5	150.90595	150.99399	151.01115
6	150.89280	151.07287	151.06376
7	151.03745	150.95455	151.05061
8	151.06376	151.04657	150.89280
9	150.98485	151.12545	151.06376
10	150.98485	151.03343	150.86649
11	150.95855	151.04657	150.91910
12	150.99800	151.13860	151.05061
13	150.90595	151.12545	150.91910
14	150.90595	151.00714	151.03745
15	150.98485	150.98085	150.87964
16	150.97170	151.04657	151.03745
17	150.94540	151.02028	150.99800
18	150.95855	150.91512	150.87964
19	151.07691	151.15174	150.85334
20	150.86649	151.15174	151.07691

Table B.3. Results for gauge length measurements at load 3 (0 kN)

Reading	Length of nominal 150 μm gauges (μm)		
	Gauge 1A	Gauge 4D	Gauge 7G
1	150.09059	149.99490	150.03799
2	150.09059	150.04749	150.05114
3	150.10374	150.02119	150.02484
4	149.89333	150.17894	150.07744
5	149.91963	150.03434	150.19580
6	150.05114	150.03434	150.10374
7	149.99854	149.94232	150.16950
8	149.94593	149.96861	150.16950
9	149.91963	150.12636	150.13005
10	149.97224	149.94232	150.16950
11	149.91963	149.96861	150.15635
12	149.91963	150.04749	150.16950
13	149.91963	150.15265	150.14320
14	149.95909	150.03434	150.11690
15	149.98539	149.96861	150.16950
16	150.10374	150.10007	150.11690
17	149.99854	150.17894	150.07744
18	149.94593	150.10007	150.09059
19	149.88018	149.92917	150.01169
20	150.13005	150.17894	149.97224

Table B.4. Results for gauge length measurements at load 4 (-252 kN)

Reading	Length of nominal 150 μm gauges (μm)		
	Gauge 1A	Gauge 4D	Gauge 7G
1	148.10482	148.03616	148.07851
2	147.94701	148.02301	148.13112
3	148.10482	148.12818	148.14427
4	148.02591	148.07560	148.07851
5	148.01276	148.00987	148.15742
6	148.01276	148.12818	148.06536
7	147.94701	148.06245	148.11797
8	148.07851	148.02301	148.11797
9	148.10482	148.07560	148.07851
10	148.07851	147.98358	148.14427
11	148.07851	148.03616	148.13112
12	148.05221	148.04931	148.01276
13	148.05221	148.07560	148.07851
14	147.99961	147.99672	148.07851
15	148.09167	148.12818	148.10482
16	147.99961	148.11504	148.11797
17	147.94701	148.04931	148.03906
18	147.96016	148.07560	148.10482
19	147.89440	148.14133	147.99961
20	147.94701	147.94414	147.98646

Table B.5. Results for gauge length measurements at load 5 (0 kN)

Reading	Length of nominal 150 μm gauges (μm)		
	Gauge 1A	Gauge 4D	Gauge 7G
1	149.17003	149.24558	149.38045
2	149.27524	149.31131	149.34100
3	149.19634	149.20615	149.34100
4	149.18319	149.14042	149.34100
5	149.22264	149.24558	149.28839
6	149.28839	149.25873	149.31469
7	149.30154	149.14042	149.27524
8	149.26209	149.15356	149.31469
9	149.18319	149.25873	149.30154
10	149.20949	149.28502	149.36730
11	149.20949	149.28502	149.38045
12	149.22264	149.25873	149.39360
13	149.17003	149.21929	149.32784
14	149.26209	149.31131	149.39360
15	149.17003	149.21929	149.32784
16	149.30154	149.23244	149.35415
17	149.20949	149.29817	149.39360
18	149.27524	149.14042	149.35415
19	149.34100	149.10098	149.23579
20	149.36730	149.16671	149.39360

Table B.6. Results for gauge length measurements at load 6 (138 kN)

Reading	Length of nominal 150 μm gauges (μm)		
	Gauge 1A	Gauge 4D	Gauge 7G
1	150.69553	150.82309	150.95855
2	150.77444	150.70478	151.03745
3	150.69553	150.86253	151.02430
4	150.85334	150.83624	151.02430
5	150.69553	150.80995	150.91910
6	150.68238	150.67849	150.98485
7	150.86649	150.71793	150.93225
8	150.82704	150.77051	150.94540
9	150.70868	150.65220	150.99800
10	150.82704	150.71793	150.86649
11	150.86649	150.79680	150.87964
12	150.76129	150.65220	150.91910
13	150.70868	150.77051	150.99800
14	150.72183	150.66534	150.90595
15	150.74814	150.80995	150.85334
16	150.76129	150.75736	150.82704
17	150.70868	150.70478	150.93225
18	150.73499	150.71793	150.85334
19	150.89280	150.86253	150.89280
20	150.87964	150.86253	150.81389

Table B.7. Results for gauge length measurements at load 7 (0 kN)

Reading	Length of nominal 150 μm gauges (μm)		
	Gauge 1A	Gauge 4D	Gauge 7G
1	149.82758	150.06063	150.06429
2	149.89333	150.08692	149.97224
3	149.93278	149.98176	150.11690
4	150.01169	149.94232	150.07744
5	149.89333	150.06063	150.02484
6	149.84073	150.07378	149.94593
7	149.97224	150.07378	150.02484
8	149.94593	149.98176	150.01169
9	150.03799	149.94232	149.95909
10	149.93278	149.96861	149.94593
11	149.90648	149.95546	150.09059
12	149.97224	149.98176	149.99854
13	149.95909	150.10007	150.09059
14	150.02484	150.07378	150.02484
15	150.01169	149.98176	150.03799
16	149.91963	149.92917	150.01169
17	149.93278	150.03434	149.98539
18	149.88018	150.06063	150.01169
19	150.03799	150.10007	150.14320
20	149.82758	149.91603	149.93278

Table B.8. Results for gauge length measurements at load 8 (-252 kN)

Reading	Length of nominal 150 μm gauges (μm)		
	Gauge 1A	Gauge 4D	Gauge 7G
1	147.13879	146.52598	146.68730
2	146.98093	146.46031	146.73984
3	147.03355	146.51285	146.70043
4	147.16510	146.43404	146.71357
5	147.15194	146.48658	146.64788
6	147.13879	146.38151	146.67416
7	147.19141	146.40777	146.64788
8	147.00724	146.53912	146.67416
9	147.13879	146.51285	146.64788
10	147.02039	146.49971	146.62161
11	147.09932	146.39464	146.62161
12	147.07301	146.38151	146.59534
13	147.19141	146.53912	146.76612
14	147.03355	146.48658	146.76612
15	147.07301	146.48658	146.63475
16	146.99408	146.47345	146.66102
17	147.03355	146.49971	146.72671
18	147.04670	146.53912	146.75298
19	147.00724	146.32897	146.56906
20	147.15194	146.34210	146.77925

Table B.9. Results for gauge length measurements at load 9 (0kN))

Reading	Length of nominal 150 □m gauges (□m)		
	Gauge 1A	Gauge 4D	Gauge 7G
1	149.30154	149.54794	149.49881
2	14 9.32784	149.39019	149.43305
3	149.34100	149.40334	149.60401
4	149.27524	149.39019	149.57771
5	149.30154	149.41648	149.47250
6	149.34100	149.41648	149.52511
7	149.34100	149.33761	149.57771
8	149.32784	149.39019	149.44620
9	149.47250	149.44277	149.59086
10	149.40675	149.37704	149.59086
11	149.38045	149.41648	149.61716
12	149.45935	149.41648	149.52511
13	149.48566	149.37704	149.52511
14	149.27524	149.45592	149.48566
15	149.35415	149.46906	149.51196
16	149.32784	149.35075	149.49881
17	149.32784	149.42963	149.45935
18	149.35415	149.52165	149.52511
19	149.51196	149.57423	149.39360
20	149.48566	149.29817	149.38045

DISTRIBUTION LIST

Microgrid Plastic Strain Analysis of a Representative F-111C Fuel Flow Vent Hole 13 Coupon

E.Kowal and M.Heller

AUSTRALIA

DEFENCE ORGANISATION

Task Sponsor AIR OIC ASI-LSA

S&T Program

Chief Defence Scientist
FAS Science Policy } shared copy
AS Science Corporate Management
Director General Science Policy Development
Counsellor Defence Science, London (Doc Data Sheet)
Counsellor Defence Science, Washington (Doc Data Sheet)
Scientific Adviser to MRDC Thailand (Doc Data Sheet)
Scientific Adviser Policy and Command
Navy Scientific Adviser (Doc Data Sheet and distribution list only)
Scientific Adviser - Army (Doc Data Sheet and distribution list only)
Air Force Scientific Adviser
Director Trials

Aeronautical and Maritime Research Laboratory

Director

Chief of Airframes and Engines Division
Research Leader Fracture Mechanics
Research Leader Structural Integrity
Research Leader Aerospace Composites

K.Watters	R.Pell
G.Clark	I.Anderson
C.Wang	K.Walker
N.Goldsmith	T.Radtke
L.Molent	E.Kowal (6 copies)
D. Holmes	M.Heller (6 copies)

DSTO Library and Archives

Library Fishermans Bend
Library Maribyrnong
Library Salisbury (2 copies)
Australian Archives
Library, MOD, Pyrmont (Doc Data sheet only)
US Defense Technical Information Center, 2 copies
UK Defence Research Information Centre, 2 copies
Canada Defence Scientific Information Service, 1 copy
NZ Defence Information Centre, 1 copy
National Library of Australia, 1 copy

Capability Systems Staff

Director General Maritime Development (Doc Data Sheet only)
Director General C3I Development (Doc Data Sheet only)
Director General Aerospace Development (Doc Data Sheet only)

Army

ABCA Standardisation Officer, Puckapunyal, (4 copies)
SO (Science), DJFHQ(L), MILPO Enoggera, Queensland 4051 (Doc Data Sheet only)

Air Force

OIC ATF ATS, RAAFSTT, WAGGA (2 copies)
CENG 501 Wing, Amberley

Intelligence Program

DGSTA Defence Intelligence Organisation
Manager, Information Centre, Defence Intelligence Organisation

Corporate Support Program

OIC TRS, Defence Regional Library, Canberra

UNIVERSITIES AND COLLEGES

Australian Defence Force Academy
Library
Head of Aerospace and Mechanical Engineering
Serials Section (M list), Deakin University Library
Hargrave Library, Monash University, (Doc Data Sheet only)
Librarian, Flinders University

OTHER ORGANISATIONS

NASA (Canberra)
Info Australia (formerly AGPS)

OUTSIDE AUSTRALIA

ABSTRACTING AND INFORMATION ORGANISATIONS

Library, Chemical Abstracts Reference Service
Engineering Societies Library, US
Materials Information, Cambridge Scientific Abstracts, US
Documents Librarian, The Center for Research Libraries, US

INFORMATION EXCHANGE AGREEMENT PARTNERS

Acquisitions Unit, Science Reference and Information Service, UK
Library - Exchange Desk, National Institute of Standards and Technology, US
National Aerospace Laboratory, Japan
National Aerospace Laboratory, Netherlands

SPARES (5 copies)

Total number of copies: **74**

DEFENCE SCIENCE AND TECHNOLOGY ORGANISATION
DOCUMENT CONTROL DATA

1. PRIVACY MARKING/CAVEAT (OF DOCUMENT)

2. TITLE

Microgrid Plastic Strain Analysis of a Representative F-111C Fuel Flow Vent Hole 13 Coupon.

3. SECURITY CLASSIFICATION (FOR UNCLASSIFIED REPORTS THAT ARE LIMITED RELEASE USE (L) NEXT TO DOCUMENT CLASSIFICATION)

Document (U)
Title (U)
Abstract (U)

4. AUTHOR(S)

E.Kowal and M.Heller

5. CORPORATE AUTHOR

Aeronautical and Maritime Research Laboratory
PO Box 4331
Melbourne Vic 3001 Australia

6a. DSTO NUMBER	6b. AR NUMBER	6c. TYPE OF REPORT	7. DOCUMENT DATE
DSTO-TR-0951	AR-011-236	Technical Report	March 2000

8. FILE NUMBER	9. TASK NUMBER	10. TASK SPONSOR	11. NO. OF PAGES	12. NO. OF REFERENCES
M1/9/453	96/102	AIR OIC ASI-LSA	47	10

URL

http://www.dsto.defence.gov.au/corporate/reports/DSTO-TR-0951.pdf

14. RELEASE AUTHORITY

Chief, Airframes and Engines Division

15. SECONDARY RELEASE STATEMENT OF THIS DOCUMENT

Approved for public release

OVERSEAS ENQUIRIES OUTSIDE STATED LIMITATIONS SHOULD BE REFERRED THROUGH DOCUMENT EXCHANGE, PO BOX 1500, SALISBURY, SA 5108

16. DELIBERATE ANNOUNCEMENT

No Limitations

17. CASUAL ANNOUNCEMENT Yes

18. DEFTEST DESCRIPTORS

Fatigue life, F-111 aircraft, Royal Australian Airforce, Airframes, Holes(openings), Strain measurement

19. ABSTRACT

This report presents results for the application and associated improvement of an AED micrograding procedure for the determination of highly localised strains. The procedure has been applied to determine plastic strains at the critical location for a plate with a reworked FFVH13 geometry, subjected to F-111C CPLT loading. By using multiple measurements over an increased gauge length of 150 μm, highly accurate strains, ranging in accuracy between 57 and 135 micro strain were determined. This accuracy level is approximately an order of magnitude better than the prior micrograding approach. For the critical region, detailed non-linear strain hysteresis responses were obtained, and the measured peak and residual strains of -2.16024% strain and -0.79349% strain respectively agreed well with prior finite element predictions. The measured residual compressive strains at the critical location indicate that there is a significant residual tensile stress, which is consistent with the known occurrence of fatigue cracking in the fleet. This investigation has also provided valuable strain data for use in validating advanced FE based constitutive models, which are currently used and under development in AED for obtaining airframe structural integrity assessments.